

# Erosion/deposition modelling on evaluating and predicting artefact assemblies

Zakynthos, Greece

R.Goudriaan

Utrecht University

Earth Sciences, department Physical Geography

Supervisor: dr. ir. G. Sterk



**Universiteit Utrecht**

Incorporated within Zakynthos Archaeology Project

### **Preface**

This thesis is my final project on the University of Utrecht and it has been by far my most intensive yet. However, I am very thankful for the manner in which I could conclude my 5,5 years of study in the Earth Sciences. The Zakynthos Archaeology Project gave me the opportunity to combine my studies with a major passion, namely archaeology.

I want to thank some people who have been very important during the fulfilment of this project.

I am very grateful to Gert Jan van Wijngaarden for his faith and support during all stages of the project. Especially his ability to give freedom and rely on the work ethics and judgement of the project contributors I found very inspirational.

I want to thank Geert Sterk, who has been my supervisor at the UU, for taking up this adventure with me and Nathan Bekkers and his valuable comments and advice. I experienced his positive attitude and willingness to help as very pleasant.

Finally I want to thank Nathan Bekkers for being the perfect field buddy and all the other people who have been working on the Zakynthos Archaeology Project for the great summer of 2009.

I want to thank IGME for allowing us to do research in their library. I want to thank EON Benelux, and than especially the laboratory department on the Maasvlakte, for their help. Finally I want to thank the Zakynthos Archaeology Project for their overall support.

The work on this thesis was intensive but interesting. I hope readers are as satisfied in reading this thesis as I was in concluding it.

### **Abstract**

Erosion/deposition was investigated on an archaeologically rich hill (Kamaroti) in southern Zakynthos, Greece. It was believed that the distribution pattern of archaeological artefacts was linked to erosion and deposition in the research area. Investigation took place by usage of a modified version of the Morgan-Morgan-Finney erosion model (MMF-model) to quantify erosion rates and look at the spatial distribution of erosion/deposition. The model was applied in a GIS-environment. Two DEM's were used, one based on interpolation of digitized 4m elevation lines, and a very detailed DEM based on differential GPS measurements.

Model results show that erosion/deposition on Kamaroti is fairly limited. This is in concurrence with results from similar types of studies on erosion/deposition in terraced olive orchards. While particle detachment by rain drop is relatively high due to the intense rainfall regime, transport capacity of the generated runoff was estimated low due the terraced layout and crop management on the hill. Artefacts are uncovered on the surface, but transportation is limited. Probably soil erosion has been limited throughout history in the entire research area. The only area where intense erosion has been taking place is probably related to human settlement in historical times.

**Table of Contents**

<b>1. INTRODUCTION .....</b>	<b>1</b>
<b>2. RESEARCH AREA .....</b>	<b>3</b>
2.1. ZAKYNTHOS .....	3
2.2. KAMAROTI.....	4
<b>3. METHODS: MORGAN-MORGAN-FINNEY EROSION/DEPOSITION MODEL.....</b>	<b>6</b>
3.1. MODEL OUTLINE.....	6
3.2. MODEL DATA COLLECTION .....	10
3.3. MODEL APPLICATION.....	14
<b>4. RESULTS AND DISCUSSION .....</b>	<b>15</b>
4.1. KAMAROTI.....	15
4.1.1. Particle detachment by rainfall .....	15
4.1.2. Runoff: Particle detachment and transport capacity .....	18
4.1.3. Soil erosion/deposition .....	21
4.2. UPPER PART OF KAMAROTI .....	25
4.3. MODEL UNCERTAINTIES .....	27
4.4. MODEL OUTPUTS VS. ARTEFACT DISTRIBUTION .....	28
<b>5. HISTORIC SOIL EROSION VS. ARTEFACT DISTRIBUTION .....</b>	<b>31</b>
<b>6. CONCLUSION .....</b>	<b>35</b>
<b>LITERATURE .....</b>	<b>36</b>
<b>APPENDICES.....</b>	<b>41</b>

### 1. **Introduction**

Zakynthos is one of the Ionian islands of Greece. It has been inhabited since the Middle Palaeolithic (late Pleistocene - early Holocene) (van Wijngaarden et al., 2005). Its strategic position, being the last seaport before entering the Mediterranean Sea, and fertile lands made sure the wealth of the inhabitants and the islands' distinguished position in various empires throughout history (e.g. the Roman Empire). Classical and Hellenistic habitation is confirmed through several historic written sources. The Roman period is attested from tombs and individual finds in Zakynthos town and on the Vassilikos peninsula, while Byzantine and Venetian times are known from monuments and written sources. The archaeological artefacts on Zakynthos consist of shards of pottery from a wide range of periods. Lithic artefacts are abundant on the island due to the presence of natural flint. The oldest remains found are Middle Palaeolithic lithics (older than 10 cal kyr BP) (van Wijngaarden, 2006). A clear archaeological record however is missing. This is probably caused by a history of natural hazards, especially soil erosion and tectonic activity (van Wijngaarden, 2006).

Zakynthos is prone to soil erosion due to a combination of steep topography and a highly erosive climate. An archaeological reconstruction simply based on the principle of superposition, where younger artefacts lie on top of older ones, is impossible. In 2007 coring in the central alluvial plain of Zakynthos led to the discovery of prehistoric artefacts at 2 meters below the present surface, while Classical shards were found at 5 meter below the surface. This indicates a serious mixing of the archaeological record due to transportation of artefacts (van Wijngaarden, 2007). It is therefore considered important to evaluate the influence of current and historic erosion/deposition on artefact distribution for correct interpretation of the archaeological record on Zakynthos.

Many studies underline the importance of geomorphologic processes on the archaeological record in general (e.g. Bintliff, 2002; Tartaron et al., 2006; James et al., 1994). Wells (2001) states that without perception of landscape evolution and geomorphologic changes the risk of misinterpreting the archaeological record is very high. In Greece many studies focussed on the occurrence of historical high erosion periods and increasing human activity throughout history (e.g. Bintliff, 2002; Fuchs, 2007; Pope & van Andel, 1984; van Andel et al., 1986). It was found that human development and the accessory increase in agricultural lands often corresponded to an increase in soil erosion in southern Greece (Fuchs, 2007). However, quantification of modern erosion/deposition patterns, their spatial distribution and incidence and impact on the archaeological remains has been subject to far less studies (James et al., 1994; Tartaron et al., 2006).

Soil erosion is a highly degrading process defined as the detachment of individual particles from soil aggregates and the subsequent transport by natural agents (Zachar, 1982). Hence, accurate quantification of modern erosion/deposition patterns can be a valuable asset for evaluating artefact origin and locating undiscovered artefact assemblies (Wells, 2001). Artefact locations unexplained by modern erosion/deposition suggests past transportation or the artefact lies in situ. Quantification of erosion/deposition patterns is usually done by modelling. Many researchers applied, modified or developed erosion/deposition models to quantify erosion at different spatial scales (e.g. Deng et al., 2008; Morgan, 2001; Vrieling et al., 2008). In this study the spatial relation between modern erosion/deposition patterns and artefact distribution on an artefact rich hill in southern Zakynthos was investigated through soil erosion/deposition modelling. Artefact distribution is strongly related to erosion and deposition. Theory states artefacts *behave* as sediments (Tartaron et al., 2006). A qualitative determination of past erosion/deposition by investigation of the geomorphologic evolution of the research area was done to clarify the distributions of artefacts which could not be explained by erosion/deposition modelling.

The goals of this research were:

- 1) to *quantitatively determine the spatial relation between present soil erosion/deposition and artefact distribution using a modified Morgan-Morgan-Finney erosion/deposition model;*
- 2) to *qualitatively determine the relation between past soil erosion/deposition and artefact distribution;*
- 3) to *investigate usefulness of soil erosion modelling for prediction of artefact assemblies;*
- 4) to *provide support on interpretation of the archaeological record and future decision making relating to the excavation of the research area.*

In general the research aimed at providing a method for determining the effects of soil erosion on artefact distribution. It helps interpretation of the finds distribution, i.e. are artefacts moved down slope or is the present artefact distribution similar to the pattern of ancient habitation? It provides support on deciding future strategies for excavation of the research area, i.e. determining locations for test trenches.

### 2. Research Area

#### 2.1. Zakynthos

Zakynthos is situated in western Greece, northwest of the Greek Peloponnesus (figure 1). It is the most southern Ionic island and has a surface area of 408 km<sup>2</sup> (Diamantopoulou & Voudouris, 2007). The island has three major areas, namely the Vrachionas mountain belt with peaks up to 800 meters in the west, the relatively flat central plain and the eastern Vassilikos peninsula (Gournelos et al., 1999; Kati & Scholle, 2008).

The western part of the island lies in the Pre-Apulian Zone and the eastern part lies in the Ionian Zone, which are the most western zones of the Hellenides (Duermeijer et al., 1999). These two zones are divided by the Ionian thrust fault (figure 1). The Pre-Apulian zone on the island consists of an eastward dipping succession of Upper Cretaceous to Miocene carbonates overlain by Pliocene-Quaternary alluvia. The Quaternary deposits consist of layers of Holocene and Pleistocene gravels, sands, silts and clays (Diamantopoulou & Voudouris, 2007). The Ionian zone consists mainly of Eocene carbonates and Pliocene sediments (Kati & Scholle, 2008).

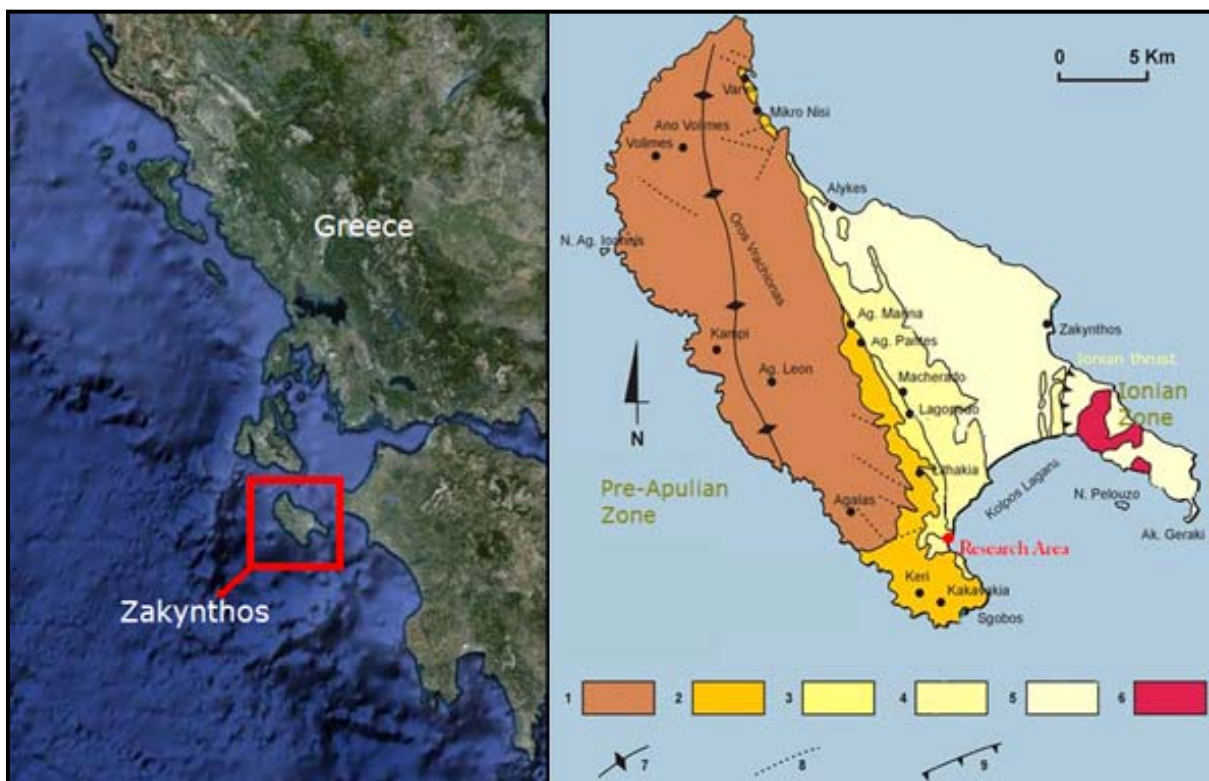


Figure 1: Left: Zakynthos is located northwest of the Greek Peloponnesus (Google Maps, 2009). Right: The geological setting of the island Zakynthos. Legend: 1. Cretaceous carbonates, 2. Eocene carbonates, 3. Oligocene marly carbonates, 4. Miocene clastics and carbonates, 5. Pliocene-Quaternary alluvial deposits, 6. Ionian evaporites and breccias, 7. Anticline 8. Fault 9. Main thrust (Ionian) (Modified after Kati & Scholle, 2008). The research area is located in the southern part of the island, northeast of Keri.

The area is considered the most seismically active in Europe. Neotectonic faulting mainly comprise NNW-SSE trending faults (Lekkas, 1993). The sedimentological evolution of the island is largely influenced by both compressional and extensional tectonics (Zelilidis et al., 1998). Subsidence and uplift have affected large parts of the coastline (Papazachos and Papazachou, 1997).

The island has a Mediterranean climate, with typical long, dry summers and torrential rains during the winter period (October-February). The mean annual precipitation over the period 1970-1997 was 826.9 mm with a standard deviation of 176 mm (weather station: 20° 54' E, 37° 47' N; altitude: 3m). Rainfall amounts range from 398 mm to 1807 mm between 1901 and 1997. (Pnevmatikos & Katsoulis, 2006). The average annual temperature is 18.0 °C. January is the coldest month (~ 9.8 °C) and August the hottest (~ 27.6 °C). The climate enables the cultivation of grapes, olives and citrus fruits. The fertile central plain is dominated by vineyards, fruit trees and olive groves. The Vrachionas mountain belt is dominated by shrubs and some coniferous forestparts. The combination of an erosive climate and steep topography makes Zakynthos vulnerable to severe water erosion. Forest fires during summer amplify erosivity of the soils. Other natural hazards occurring include earthquakes, landslides, rock fall and floods (Theodoros et al., 1997).

### **2.2. Kamaroti**

The research area is located on the artefact rich hill Kamaroti which is located in the southern part of the island, northeast of Keri (figure 1). The area was chosen because of the high amount of surface finds and the suggested influence of modern erosion/deposition on artefact scatter. Surface finds consist of shards of pottery ranging from the Early Bronze Age until modern time. Palaeolithic flints are scarce. Coring uncovered multiple archaeological artefacts including Mycenaean pottery shards and other Early to Late Bronze Age material.

Kamaroti is ellipse shaped with the major axis running NE-SW and has a maximum height of 86 meter. The northern slopes are relatively steep ( $\pm 20^\circ$ ). The S-SE slope is relatively gentle ( $\pm 10^\circ$ ), around 400 meters long and descends to sea level. The hill consists of Miocene limestone covered by Holocene sediments (Kati & Scholle, 2008). The top has an upper layer of silty loams/silty clay loams covering clays. Shallow soils of silty loams/silty clay loams/sandy clays cover bedrock on the northern and western slopes. The E-SE part has no or shallow silty loam/silty clay loam leptosols covering limestone bedrock. Preceding westwards along the S-SE slope shallow soils of silty clay loams on sandy clays cover the limestone bedrock. The southern slope has deeper soils of clays

covered by sandy clays. The ground surface shows a lot of mudcracks on the S-SE slopes.

The climate is comparable to the rest of the island. Land use on Kamaroti consists mostly of terraced olive groves under different grades of maintenance. Historic aerial photographs show that these terraces have been made between 1986 and 1993. The northern slope consists of ploughed bench terraces with olives and without undergrowth. The western slope consists of ploughed terraces with olives and without undergrowth proceeding downhill into terraces with olives and a lot of undergrowth. The eastern slope is camping terrain. The south-eastern slope has ploughed terraces with olives without undergrowth on top. Preceding downwards an area consisting of ancient terraces/structures with much undergrowth and stone cover is found, leading into well maintained, ploughed, terraces, without undergrowth downhill. The eastern part of the south-eastern slope is considerably rockier than the western part.

The area used in this study is located on the S-SE slope of Kamaroti (figure 2). The research area is a relatively closed system, bordered in the northeast by a rocky area, the east consists of seaside cliffs, and the west by a former brook. The 68400 m<sup>2</sup> research area is around 450 m long and 150 m wide with a height difference of  $\pm 80$  m.

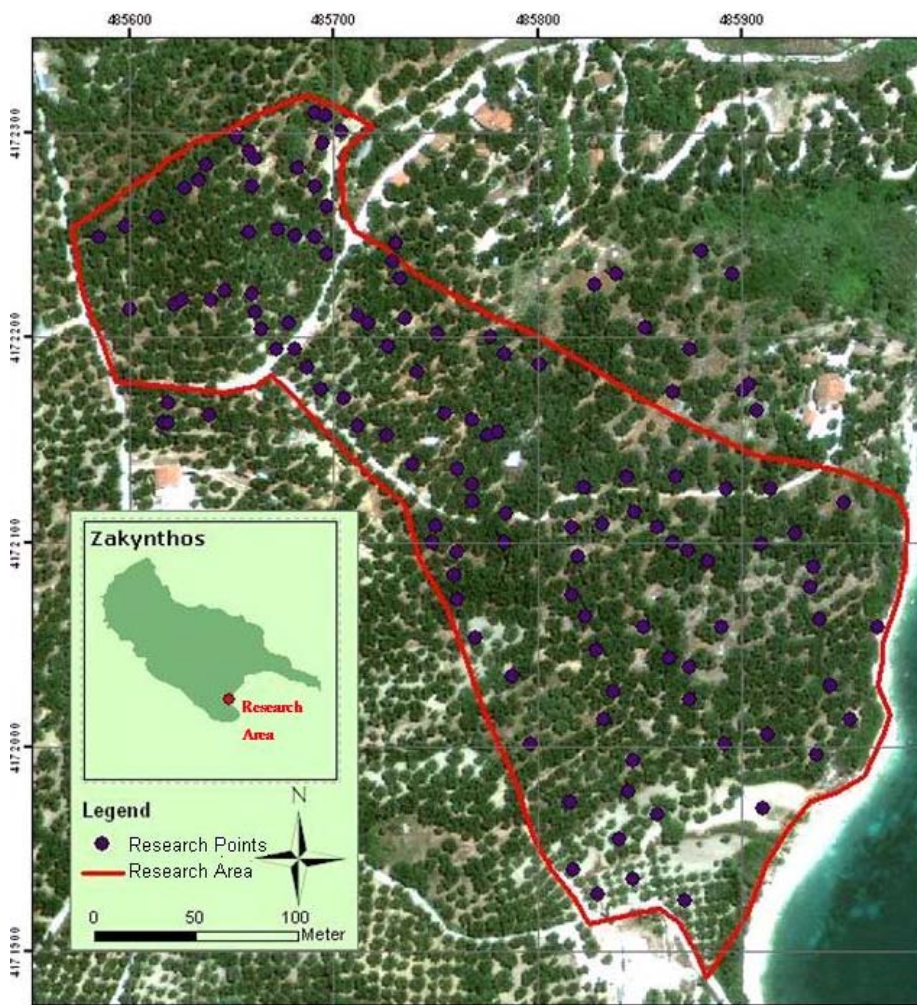


Figure 2: The research area.

### 3. Methods: Morgan-Morgan-Finney Erosion/Deposition Model

MMF-model is a relatively simple conceptual model used to predict soil erosion and deposition on a field scale. A conceptual model reflects the physical processes governing a system, but describes them with empirical relationships (Saavedra, 2005). Parameter inputs are based on topography, climatic conditions, hydrology, vegetation and soil properties (Morgan, 1984). The MMF model is an annual model which has been successfully used at plot, hill slope and catchment scales in a wide range of environments. A modified version of the Morgan-Morgan-Finney erosion/deposition model (MMF-model) was used to quantify erosion rates (figure 3) (Morgan, 2001).

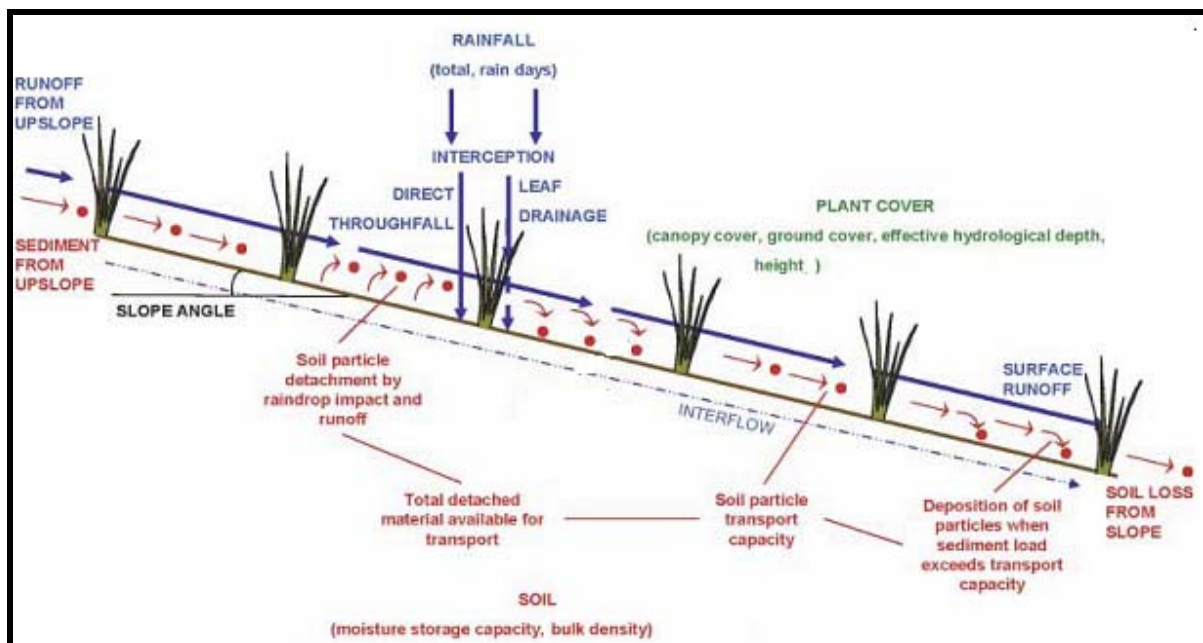


Figure 3: Schematic representation of the steps used in the MMF-model (after Morgan & Duzant, 2008).

#### 3.1. Model Outline

The following section gives an overview of the main equations used in the MMF model. All parameters with a subscript  $m$  (1-12) are calculated per month. Variables lacking a subscript  $m$  are calculated per year.

##### *Particle detachment by rainfall*

Rainfall kinetic energy determines the maximum possible detachment of soil particles by splash erosion (Morgan, 2001). The model starts by calculating the effective rainfall  $RF_m$  (mm), as the mean monthly rainfall  $R_m$  (mm) minus permanent interception by the vegetation cover ( $PI$ ; 0-1):

$$RF_m = R_m (1 - PI) \quad (1)$$

The effective rainfall is divided in direct throughfall ( $DT_m$ ; mm) and leaf drainage ( $LD_m$ ; mm). Leaf drainage consists of water reaching the soil surface as flow or drips from leaves and stems. The amount of leaf drainage directly depends on the proportion of effective monthly rainfall intercepted by the (olive tree) canopy cover ( $CC$ ; 0 – 1):

$$LD_m = RF_m CC \quad (2)$$

Direct throughfall hits the ground surface uninterrupted by the vegetation cover. It consists of the effective rainfall minus the leaf drainage:

$$DT_m = RF_m - LD_m \quad (3)$$

Total kinetic energy of the direct throughfall ( $KEDT_m$ ;  $J m^{-2}$ ) depends on rainfall intensity  $I$  ( $mm h^{-1}$ ).  $KEDT_m$  was determined using a relation found for central Italy which is assumed suitable for Mediterranean-type climates (Zanchi and Torri, 1980):

$$KEDT_m = (9.81 + 11.25 \log_{10} I) DT_m \quad (4)$$

The kinetic energy of leaf drainage ( $KELD_m$ ;  $J m^{-2}$ ) is a function of tree canopy height ( $PH$ ; m) as proposed by Brandt (1990):

$$KELD_m = [(15.80 PH^{0.5}) - 5.875] LD_m \quad (5)$$

The total kinetic energy of rainfall ( $KET_m$ ;  $J m^{-2}$ ) is the sum of the kinetic energy from leaf drainage and direct throughfall:

$$KET_m = KEDT_m + KELD_m \quad (6)$$

Soil detachment by raindrops ( $F_m$ ;  $kg m^{-2}$ ) is calculated from:

$$F_m = 10^{-3} K KET_m (1 - GC_m) \quad (7)$$

where  $GC_m$  (0-1) is ground cover by non-erodible material (ground vegetation, rocks, crop residues) and  $K$  ( $g J^{-1}$ ) is the soil detachability index from the Revised Universal Soil Loss Equation (Svorin, 2003). The main properties affecting  $K$  are soil texture, organic matter, structure and permeability of the soil profile (Yue-Qing et al., 2008), leading to the following formula of Wischmeier & Smith (1978) with a minimum of  $K = 0$ :

$$K = [2.1 \cdot 10^{-4} (12-OM) M^{1.14} + 3.25 (SS-2) + 2.5 (PE-3)] / 100 \quad (8)$$

in which  $M$  is:

$$M = (\% \text{ silt} + \% \text{ fine sand}) (100 - \% \text{ clay}) \quad (9)$$

and  $OM$  (%) is the organic matter content of the soil.  $SS$  (-) is the soil structure code and  $PE$  (-) the permeability class from the RUSLE model.

Yearly soil detachment by raindrop  $F_{yr}$  ( $\text{kg m}^{-2}$ ) is calculated through:

$$F_{yr} = \sum_{m=1}^{12} F_m \quad (10)$$

*Runoff: particle detachment and transport capacity*

The mean rainfall per rain day  $RD$  (mm) is the mean yearly rainfall  $R$  (mm) divided by the mean number of rainy days per year  $RN$  (-):

$$RD = R / RN \quad (11)$$

Runoff occurs where the mean rainfall per day  $RD$  exceeds the soil moisture storage capacity  $SC$  (mm) (Kirkby, 1976). The soil moisture storage capacity is depending on the gravimetric soil moisture content at field capacity ( $MS$ ; %); the dry bulk density of the soil ( $BD$ ;  $\text{Mg m}^{-3}$ ); the effective hydrological depth of the soil (EHD; m), indicating the depth of soil within which the moisture storage capacity controls generation of surface runoff; and the ratio of actual over potential evapotranspiration ( $Et/Eo$ ; -):

$$SC = 1000 MS BD EHD (Et/Eo)^{0.5} \quad (12)$$

The runoff generated in a grid cell that does not receive runoff from a neighbouring cell ( $QR$ ; mm) is calculated using:

$$QR = RF_{yr} \exp(-SC / RD) \quad (13)$$

For cells that receive rainfall and incoming surface runoff the total surface runoff is calculated as:

$$QS = (RF_{yr} + Q_{ce}) \exp(-SC / RD) \quad (14)$$

in which  $RF_{yr}$  (mm) is the yearly effective rainfall and  $Q_{ce}$  (mm) is the runoff contribution from elements upslope following the local drainage pattern. This equation allows re-infiltration of a part of the surface runoff along the hill slope.

Soil particle detachment by surface runoff ( $H$ ;  $\text{kg m}^{-2}$ ) is estimated through:

$$H = 10^{-3} QS^{1.5} \sin(S) (1-GC) (0.5 COH)^{-1} \quad (15)$$

where  $COH$  (kPa) is cohesion of the soil,  $S$  is slope ( $^\circ$ ) and  $QS$  is total surface runoff.

The transport capacity of runoff ( $TC$ ;  $\text{kg m}^{-2}$ ) is estimated by:

$$TC = 10^{-3} C P QS^2 \sin(S) \quad (16)$$

where the cover management ( $C$ ; -) and support practice factor ( $P$ ; -) are the same as in the Revised Universal Soil Loss Equation (RUSLE).

### *Soil erosion/deposition estimation*

For each cell potential erosion  $E$  ( $\text{kg m}^{-2}$ ) is the sum of soil particle detachment by surface runoff ( $H$ ) and impact of raindrops ( $F_{yr}$ ) (Pfeffer, 2003):

$$E = H + F_{yr} \quad (17)$$

Soil erosion/deposition amount per cell is the sum of particle detachment by raindrop and surface runoff limited by the transport capacity. The following formula gives the erosion/deposition rate  $E_{OUT}$  ( $\text{kg m}^{-2}$ ) per cell when there are no upstream cells (Pfeffer, 2003):

$$E_{OUT} = \min(E, TC) \quad (18)$$

The eroded material is transported downstream through the local drainage pattern. The amount of eroded material received by the lowest neighbour cell ( $E_{IN}$ ;  $\text{kg m}^{-2}$ ) is calculated through (Pfeffer, 2003):

$$E_{IN} = \sum_{i=1}^n E_{OUT}(S_i) \quad (19)$$

where  $S_i$  are neighbouring upstream cells, with a maximum of  $n=7$ . The erosion/deposition rate  $E_{OUT}$  when there is addition of soil from upstream cells is calculated using:

$$E_{OUT} = \min[(E + E_{IN}), TC] \quad (20)$$

For each cell, net erosion per year ( $E_{net}$ ;  $\text{kg m}^{-2} \text{yr}^{-1}$ ) is (figure 4) (Pfeffer, 2003):

$$E_{net} = E_{IN} - E_{OUT} \quad (21)$$

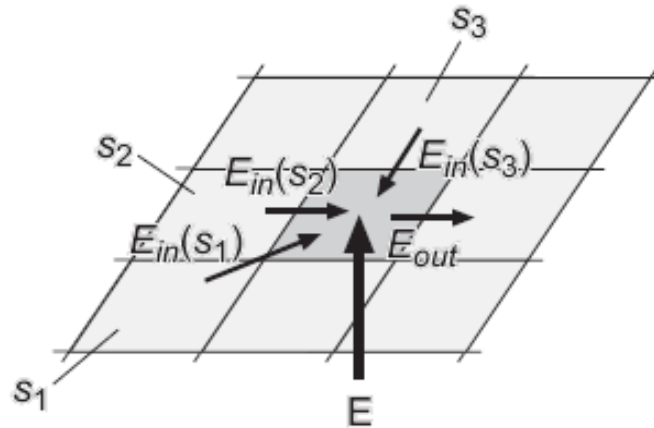


Figure 4: Total net erosion per year  $E_{net}$  ( $\text{kg m}^{-2} \text{yr}^{-1}$ ) is determined by potential erosion  $E$ , transport out of the cell  $E_{OUT}$  and transport into the cell  $E_{IN}$ . The maximum of neighbouring upstream cells is 7 (Pfeffer, 2003).

### 3.2. **Model Data Collection**

The required input parameters for the MMF-model are listed in table 1. Measured values were used if possible, otherwise guide values from literature were used. Fieldwork took place from 15<sup>th</sup> of June 2009 until the 1<sup>st</sup> of August 2009. A second period of fieldwork took place from 12 until 19 October 2009. During the summer and October campaign input parameter values concerning soil characteristics and vegetation cover were measured or estimated. Vegetation parameters estimated in summer were assumed valid for the dry season (April-September) while vegetation parameters estimated in October were assumed valid for the wet season (October-March). Parameter values were collected at 127 research points distributed over the research area (figure 2). Soil samples (107) were taken on most of these points. Research point locations were based on identifiable topographical features in the field. At least one point was taken on each agricultural terrace with an increasing amount of points according to the heterogeneity of the terrace. The point locations were mapped in ArcGIS using GPS-coordinates ( $\pm 4\text{m}$ ). Point locations were corrected if necessary based on field photographs and satellite imagery (Geoeye from 10 May 2009). Inversed distance weighting in ArcGIS was used to predict parameter values for the entire area. All input and output maps have a spatial resolution of  $0.5 \text{ m} \times 0.5 \text{ m}$ .

## Erosion/deposition modelling on evaluating and predicting artefact assemblies

Table 1: Input parameters of the MMF-model (Based on Morgan & Duzant, 2008; Morgan, 2001).

Factor	Variable	Definition	Way of Acquirement
Topography	S	Slope steepness ( $^{\circ}$ )	Derived from of DEM
Climate	$R_m$	Mean monthly rainfall (mm)	Zakynthos weather station
	$RN_m$	Mean monthly number of rain days (-)	Zakynthos weather station
	I	Typical intensity of erosive rain ( $\text{mm h}^{-1}$ )	Morgan & Duzant, 2008
Land Cover	CC	Tree canopy cover expressed as the proportion of the soil surface (0-1)	Field estimation
	PI	Permanent interception expressed as the proportion of rainfall (0-1)	$0.217 \times CC$ (Gómez et al., 2001)
	$GC_m$	Ground cover expressed as a proportion of the soil surface (0-1)	Field estimation
	PH	Plant height (m)	Field estimation
	$C_m$	Cover management factor of the Revised Universal Soil Loss Equation(-)	Table 2, reclassification of ground- and canopy cover maps
	P	Support practice factor of the Revised Universal Soil Loss Equation (-)	Table 3, reclassification of slope map S
	$Et/Eo_m$	Ratio of actual over potential evapotranspiration (0-1)	Estimated using Cropwat model
	ST	Percentage rock fragments on soil surface (0-1)	Field estimation
Soil	MS	Soil moisture at field capacity (% w/w)	Table 4, based on grain size distribution
	BD	Bulk density of top soil layer ( $\text{Mg m}^{-3}$ )	Table 4, based on grain size distribution
	EHD	Effective hydrological depth of the soil (m)	Based on type of (vegetation) ground cover
	COH	Cohesion of the surface soil (kPa)	Table 4, based on grain size distribution
	OM	Organic matter (%)	Based on loss on ignition
	SS	Soil structure code (-)	Based on field estimation
	PE	Permeability class (-)	Table 4, based on grain size distribution
	GSD	Grain size distribution	Grain size analysis of soil samples

During the October campaign differential GPS (DGPS) points were taken from the upper part of the research area. Through interpolation by ordinary kriging in ArcGIS a highly detailed digital elevation model (DEM) of this part was developed. The fill option in ArcGIS made sure no sinks were present in the data. A DEM of the entire research area was created by interpolation of contour lines from a topographic map from 1970. Contour intervals are 4 meters. The developed DEM was partly verified by comparison to the DGPS points. Slope (S) was derived from both DEM's. The local drainage pattern was found through the *flow direction* tool in ArcGIS.

Average monthly rainfall values ( $R_m$ ; mm), average monthly number of rain days ( $RN_m$ ; -) and average monthly temperature ( $^{\circ}\text{C}$ ) were attained from 1970-2000 climate data of the weather station near Zakynthos airport ( $20^{\circ} 54' \text{ E}$ ,  $37^{\circ} 47' \text{ N}$ ; altitude: 3m;  $\pm 5 \text{ km}$  northeast of research area). Erosive rainfall intensity  $I$  was assumed  $30 \text{ mm h}^{-1}$  for Zakynthos' strongly seasonal climate (Morgan & Duzant, 2008). The obtained climatic parameter values were assumed valid and similar for the entire research area. Input maps for the MMF-model were developed in ArcGIS.

Tree canopy cover ( $CC$ ; 0-1) was based on visual estimations at the research points. Interpolation through inversed distance weighting delivered the input map for the MMF model. Many combinations of input variables (power, maximum distance of research points, maximum number of research points) for the inversed distance calculation were tried. The resulting  $CC$  maps were visually compared with the Geoeye (10 may 2009) satellite imagery of the area. The best result was chosen as the  $CC$  input map for the MMF-model (power: 4, max. distance of research points: 45m, max. nr. of research points: 3) and used to calculate all other input maps of land cover variables. The permanent interception map ( $PI$ ; 0-1) was calculated through multiplication of  $PI$  for olive trees (0.217; Gómez et al., 2001) with the  $CC$  input map. Plant height ( $PH$ ; m) was based on visual estimations of the mean height of the lowest leaves at the research points. Interpolation of these point estimations resulted in the  $PH$  input map. Groundcover  $GC_m$  (0-1) was visually estimated in the field in the summer and in October at the research points. Groundcover in the summer months was based on estimations on stone cover  $ST$  (0-1) and vegetation ground cover. Groundcover in the winter months was based only on vegetation because of the high coverage in the wet period. Interpolation of these point estimations resulted in the  $GC_m$  input map. The roads in the research area were digitized and have a standard  $GC_m$  of 1. The yearly ratio of actual over potential evapotranspiration ( $Et/E_o$ ; 0-1) was estimated with the FAO Cropwat-model. Estimations were done using yearly temperature, yearly rainfall and vegetation cover parameters. The  $Et/E_o$ -value was assumed similar in the entire research area.

Table 2: Cover management values ( $C$ ) for Mytilini, Lesvos (modified after Arhonditsis et al., 2002).

Olive Groves	C
Tree Canopy	
> 60%	0.008 ± 0.002
30 – 60%	0.012 ± 0.003
< 30%	0.020 ± 0.004
Ground Cover	
> 50%	0.005 ± 0.002
20 - 50%	0.010 ± 0.002

Table 3: Erosion control practice factors ( $P$ -factor) for Mytilini, Lesvos (Arhonditsis et al., 2002).

Terracing: Slope $S$ (%)	P
$S \leq 5$	0.20 ± 0.01
$5 < S \leq 10$	0.25 ± 0.02
$10 < S \leq 15$	0.30 ± 0.02
$15 < S \leq 20$	0.35 ± 0.01
$20 < S \leq 25$	0.45 ± 0.01
$25 < S \leq 30$	0.55 ± 0.03
$30 < S \leq 35$	0.70 ± 0.02
$35 < S$	1.00 ± 0.02
No Erosion Control Practices	1.00

Cover management factors ( $C$ ; 0-1) and support practice factors ( $P$ ; 0-1) were based on a study by Arhonditsis et al. (2002) in Mytilini (tables 2 and 3).  $C$  was based on the way of cultivation of olive groves which was determined with the summer and winter ground vegetation cover map ( $GC_m$ ) and the canopy cover map ( $CC$ ). If ground vegetation coverage exceeds 20% these percentages were reclassified according to table 2. Otherwise reclassification took place following the tree canopy cover map. The resulting cover management maps for summer and winter conditions were added and divided by two to give the yearly cover management factor. Roads got a standard  $C$  of 1.

Terracing is found all over the area. The support practice factor was based on the slope according to table 3. Roads got a standard  $P$  of 1.

Table 4: Input values for different soil types for MMF-model (Morgan & Duzant, 2008; Morgan, 2001; Lopez-Vicente & Navas, 2005).

Soil type	MS	BD	COH	PE
Sand	0.08	1.5	2	1
Loamy sand	0.15	1.4	2	2
Sandy loam	0.28	1.2	2	2
Loam	0.20	1.3	3	3
Silt	0.15	1.3	-	3
Silt Loam	0.35	1.3	3	3
Sand clay loam	0.38	1.4	3	4
Clay loam	0.40	1.3	10	4
Silty clay loam	0.42	1.3	9	5
Sandy clay	0.28	1.4	-	5
Silty clay	0.30	1.3	10	6
Clay	0.45	1.1	12	6

Dry bulk density ( $BD$ ;  $Mg\ m^{-3}$ ), gravimetric soil moisture content ( $MS$ ; %w/w), surface soil cohesion ( $COH$ ; kPa) and permeability class ( $PE$ ; -) were estimated following Morgan & Duzant (2008) and Lopez – Vicente et al. (2005) (table 4). The permeability class  $PE$  represents the degree of saturated hydraulic conductivity of a soil and is based on soil texture (Lopez-Vicente et al., 2005). Also  $BD$ ,  $COH$  and  $MS$  values were based on soil texture ( $GSD$  = Grain size distribution). Soil texture was determined using the USDA soil texture triangle after grain size analysis on 59 soil samples from the top soil (Konert & Vandenberghe, 1997; Appendix I). Sample locations were chosen to give a good coverage of the research area. The obtained parameter values were interpolated using inversed distance weighting (power: 3, max. distance of research points: 50m, max. nr. of research points: 4) to provide input maps for the MMF-model. Organic matter content ( $OM$ ; %) was based on loss of ignition of all 107 soil samples.  $OM$  values were interpolated following the same scheme as the vegetation parameters. Effective hydrological depth  $EHD$  (m) is based on vegetation cover and the presence of surface crusts.  $EHD$  is 0.5m when surface crusts are present and without surface crusts  $EHD$  is estimated 0.1m. Roads have an  $EHD$  of 0 (Morgan & Duzant, 2008). The soil structure

code *SS* represents the type of aggregate structure of the soil. Four types of aggregate structures are distinguished: very fine granular (<1 mm; *SS* = 1), fine granular (1 – 2 mm; *SS* = 2), medium or coarse granular (2 – 10 mm; *SS* = 3) and blocky, platy or massive (>10 mm; *SS* = 4) (Lopez-Vicente et al., 2005). Most of the soils in the research area have a platy aggregate structure. It was therefore assumed that *SS* = 4 in the entire research area.

### 3.3. **Model Application**

Modelling was done in ArcGIS (appendix II). The research area was divided into grid cells of 0.5 m x 0.5 m and for each grid cell annual soil erosion/deposition was calculated. Detachment by raindrop *F* was calculated per month since variation in monthly rainfall quantities and vegetation ground cover on Zakynthos is high. In the end this was summed to yearly values. Detachment by runoff *H* and transport capacity *TC* were calculated using yearly values. Erosion/deposition *E<sub>net</sub>* was also calculated based on yearly parameter values.

The MMF-model was applied at two scales. Erosion/deposition on the upper part of the research area was modelled using a very precise DEM based on point elevations from differential GPS with a high density of measurement points. Erosion/deposition was estimated for the entire research area based on a DEM from digitized contour lines with a height resolution of 4 meters. The model was run twice for both scales, once with the assumption that no surface sealing occurs in the area and once with the assumption that surface sealing occurs all over the area. Surface sealing influences the effective hydrological depth of the soil. According to Morgan & Duzant (2008) soils with a surface crust have an *EHD* of 0.5m, while soils without a surface crust have an *EHD* of 0.1m.

The model results were compared with artefact scatter maps provided by the archaeological team. The archaeological data was delivered by the Zakynthos Archaeology Project (ZAP) (appendix III). Evaluation of the artefact distribution was done by visual comparison of the model outputs with the archaeological maps. Furthermore correlation matrices were used to investigate possible correlation between artefact scatter with various model parameters/outputs.

#### 4. Results and Discussion

##### 4.1. Kamaroti

##### 4.1.1. Particle detachment by rainfall

The average monthly rainfall over the period 1970-2000 was 69 mm divided over 6.8 rain days. Rainfall amounts on Zakynthos are particularly high from October until March. Between 1970 and 2000 an average of 86% of the yearly total rainfall was recorded in this period. November is the wettest month with an average monthly rainfall of 142.5 mm and June the driest month with an average of 5.2 mm. The number of rain days per month is highest in November (average of 12.5) and lowest in July (average of 0.3).

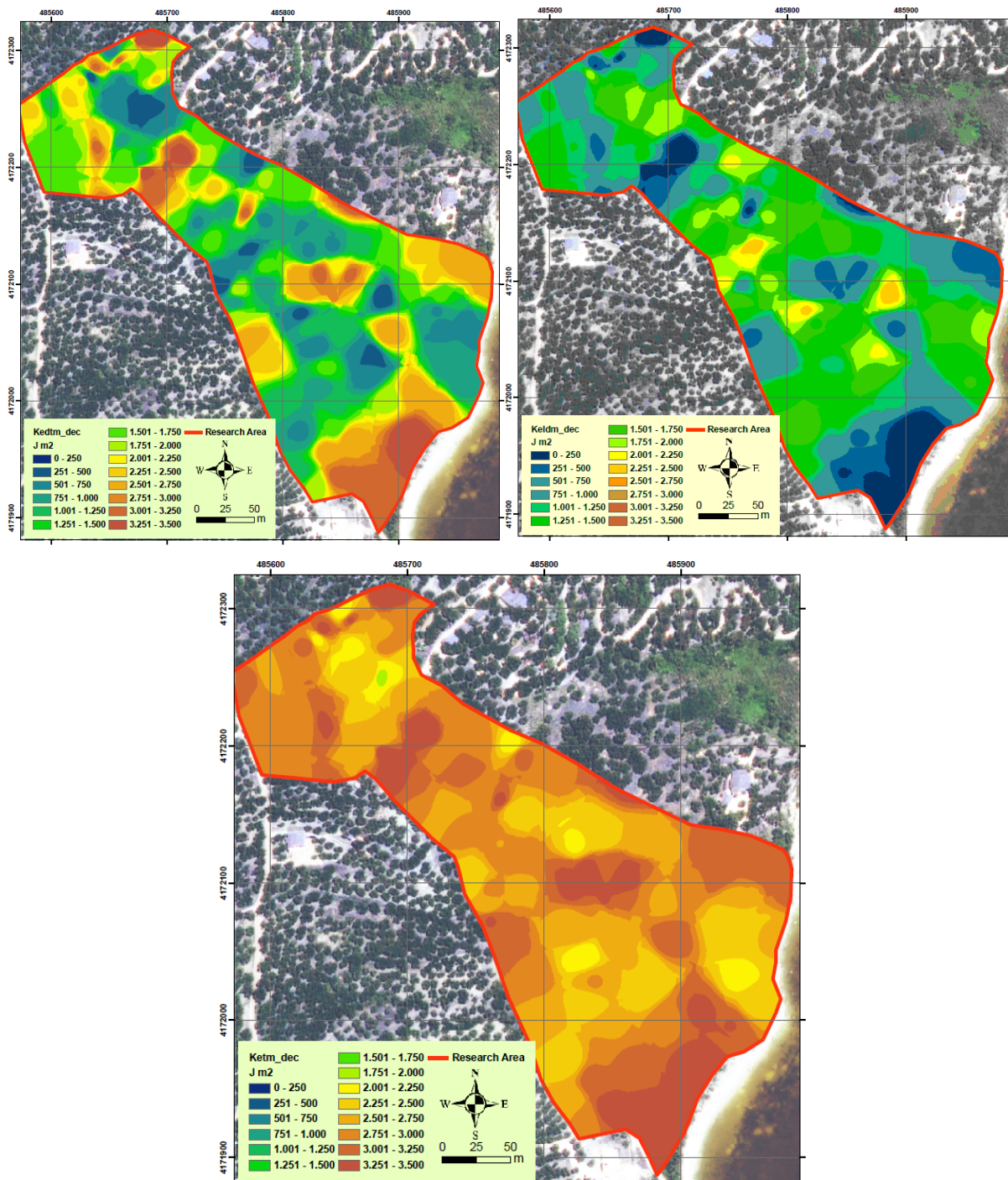


Figure 5: Up left: Kinetic energy of direct through fall in  $J m^2$  in December. Up right: Kinetic energy of leaf drainage in  $J m^2$  in December. Below: Total kinetic energy of rainfall in  $J m^2$  in December.

Tree canopy cover was estimated at 47.3 % for the research area. After taking account for permanent interception and tree canopy cover, direct through fall is highest in the most southern part of the area where the olive trees are still young and provide less cover. The spatial distribution of direct through fall amounts remains the same throughout the year, although quantities vary. This is a logical consequence of the small variation in canopy cover of olive trees and the high variation in monthly rainfall amounts. Leaf drainage (LD; mm) amounts logically show a distribution pattern inverted to direct through fall. Total kinetic energy per year over the entire research area was an estimated average of  $17628 \text{ J m}^{-2}$  with a standard deviation  $2087 \text{ J m}^{-2}$ . Minimum rainfall energy was  $12113 \text{ J m}^{-2}$  and maximum  $21852 \text{ J m}^{-2}$ . These values are quite similar to values found in literature for Mediterranean areas (Badia & Marti, 2008). Quantities differ due to varying canopy cover. An estimated 60% of the total kinetic rainfall energy in the research area comes from direct through fall ( $\text{KEDT}_m$ ;  $\text{J m}^{-2}$ ) and 40 % from leave drainage ( $\text{KELD}_m$ ;  $\text{J m}^{-2}$ ) (while tree canopy cover is 47.3 %). Total rainfall energy is highest in November and lowest in June. Figure 5 shows the KE distributions in December.

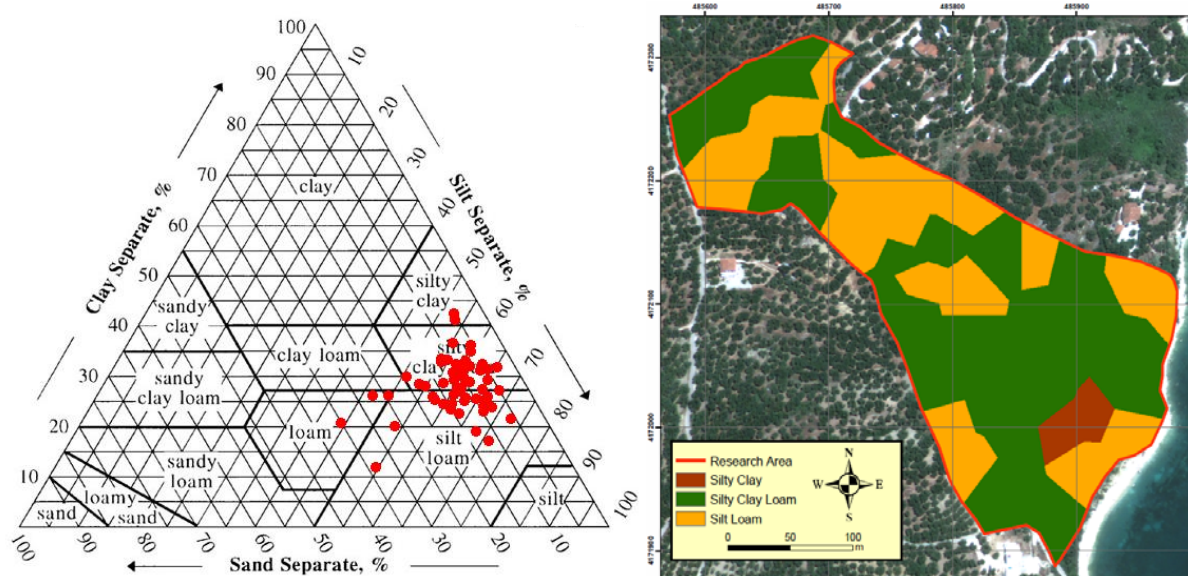


Figure 6: Soil textures and distribution based on grain size analysis.

The 59 soil samples mainly consisted of silty clay loam (33) and silt loam (21). The remaining samples consisted of silty clay (2) and loam (3). The three loam samples are considered invalid because of probable overestimation of the sand fraction. Soil parameters were estimated after the grain size analysis results and their spatial distribution was correlated to the soil types (figure 6). The bulk density of the top soil ( $BD$ ;  $\text{Mg m}^{-3}$ ) is 1.3 in the entire research area based on the grain size distributions. Silty clay loams have a soil moisture at field capacity  $MS$  (% w/w) of 0.42, a permeability

class  $PE$  (-) of 5 and a cohesion factor  $COH$  (kPa) of 9. Silt loams have a  $MS$  of 0.35,  $PE$  of 3 and  $COH$  of 3. Silty clays have a  $MS$  of 0.30,  $PE$  of 6 and  $COH$  of 10. Soil detachability index  $K$  ( $g J^{-1}$ ) varies between 0 and 0.45 with an average of 0.29 and a standard deviation of 0.09.

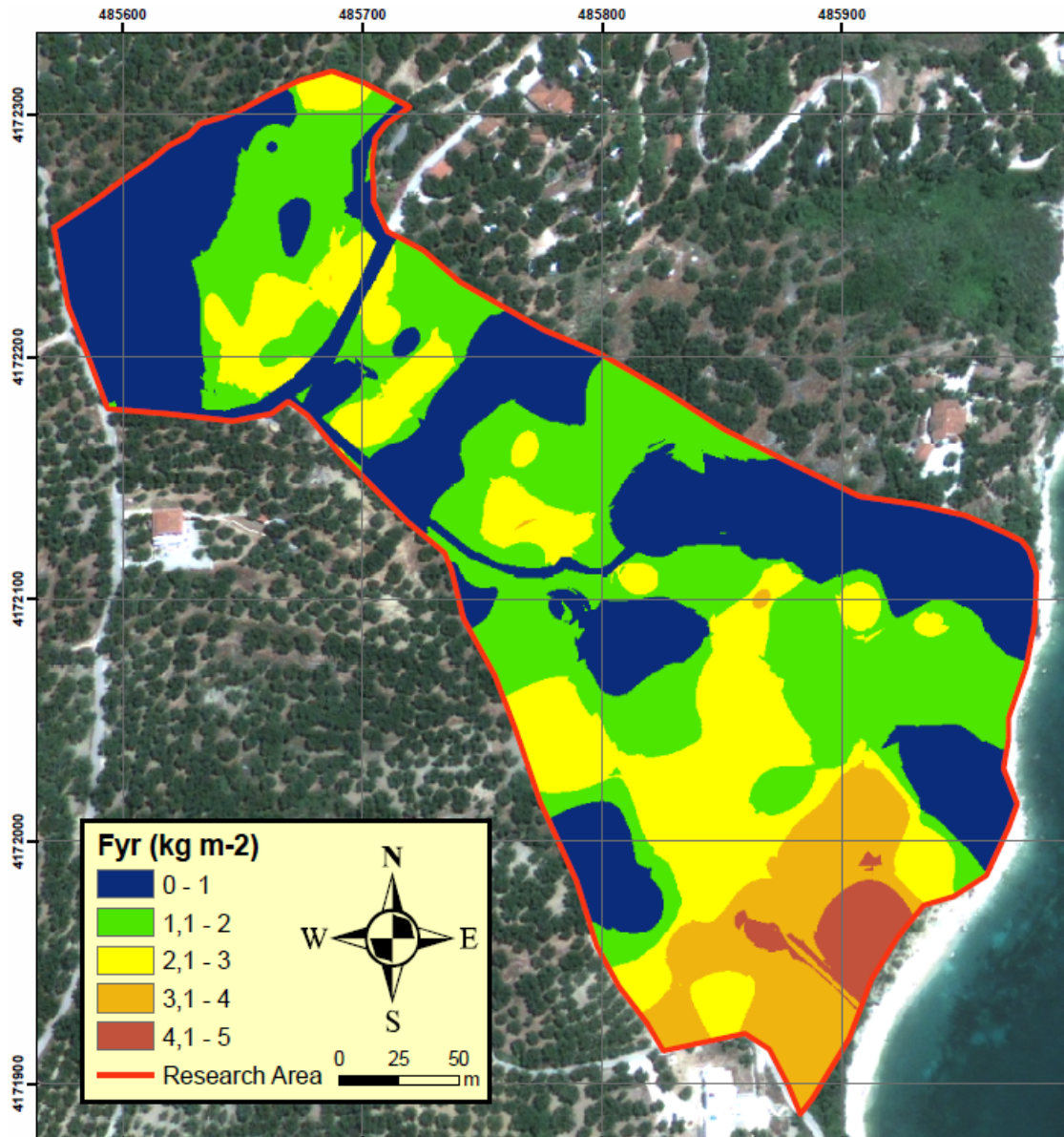


Figure 7: Total detachment ( $F$  in  $kg\ m^{-2}\ yr^{-1}$ ) for the entire research area.

Ground cover varies heavily during the year. The vegetation ground cover is depleted by the summer drought but recovers quickly after the first winter precipitation. Average vegetation ground cover was estimated at 45.2% in the dry season and 74.7% in the wet season in the entire research area. With addition of stone cover in the summer month's average ground cover was estimated equal to 52.5%. The average groundcover per year was estimated at 64% of the entire research area. Particle detachment by rainfall  $F_{yr}$  ( $kg\ m^{-2}$ ) logically is highest where ground cover is lowest. In the wet season 71.3% of the total detachment per year takes place against 28.7% in the dry season (figure 7).

November has the highest particle detachment with an estimated average of  $0.23 \text{ kg m}^{-2}$  for the entire research area and June the lowest with an estimated average of  $0.02 \text{ kg m}^{-2}$ . The estimated average amount of particle detachment in the research area is  $1.54 \text{ kg m}^{-2} \text{ yr}^{-1}$  with a standard deviation of  $1.11 \text{ kg m}^{-2} \text{ yr}^{-1}$ . Minimum detachment is  $0.00 \text{ kg m}^{-2} \text{ yr}^{-1}$  and maximum detachment is  $4.81 \text{ kg m}^{-2} \text{ yr}^{-1}$ . In the research area an estimated 105.2 tons of soil is detached through rain drops per year. The spatial distribution of severity of  $F_{yr}$  as estimated by the model is very much in accordance to expectations based on the fieldwork.

### 4.1.2. Runoff: Particle detachment and transport capacity

The ratio of actual over potential evapotranspiration  $Et/Eo$  (-) was estimated at 0.62 for the entire year and 0.59 during the growth season of olives (February-October). From November until April the abundant rainfall between October and March supplies enough water for evapotranspiration ( $Et/Eo = 1.00$ ). Between May and September high temperatures and low rainfall amounts result in drought. Although the average monthly rainfall amounts increase drastically in October, low soil moisture contents still reduce the actual evapotranspiration ( $Et/Eo = 0.83$ ).

Average rainfall per year  $R$  is 826.9 mm separated over 81.6 rain days. This means an average of 10.1 mm of rain per rain day ( $RD$ ; -). The mean effective rainfall per year is 742.0 mm. When  $EHD$  was estimated 0.1m (no surface sealing) the soil moisture storage capacity ( $SC$ ; mm) of the soil varies between 0.0 mm (road) and 43.0 mm, with an average of 38.6 mm. The runoff per grid cell generated by precipitation,  $QR$  (mm) has an average of 38.8 mm and a standard deviation of 132.9 mm. In the olive groves the mean amount of runoff per year is estimated 15.3 mm with a standard deviation of 5.4 mm. The highest amount generated is 38.2 mm and the lowest 9.6 mm of runoff. On the road the highest amounts of runoff are generated per year (estimated mean: 744.0 mm). The average total surface runoff  $QS$  (mm), apart from main stems, in the olive orchards is 15.9 mm, with a standard deviation of 10.0 mm (figure 8). Main stems are defined as raster cells with a stream order higher than 30 according to the method of Shreve (1967). Runoff through these main stems was not estimated. In the erosion/deposition part of this chapter (§ 4.1.3) this choice will be further elucidated.

Detachment by runoff  $H$  is estimated much lower in the olive orchards than detachment by raindrop  $F$  with an estimated average of  $0.00046 \text{ kg m}^{-2}$  (outside main stems) and a standard deviation of  $0.00629 \text{ kg m}^{-2}$ . The spatial distribution of  $H$  is mainly the result of the combination of ground cover  $GC$  and cohesion  $COH$ .  $TC$  has an estimated average of  $0.00031 \text{ kg m}^{-2}$  with a standard deviation of  $0.0042 \text{ kg m}^{-2}$ . Transport capacities are high on the road, but low in the olive orchards as a result of terracing and the crop management factor  $C$ .

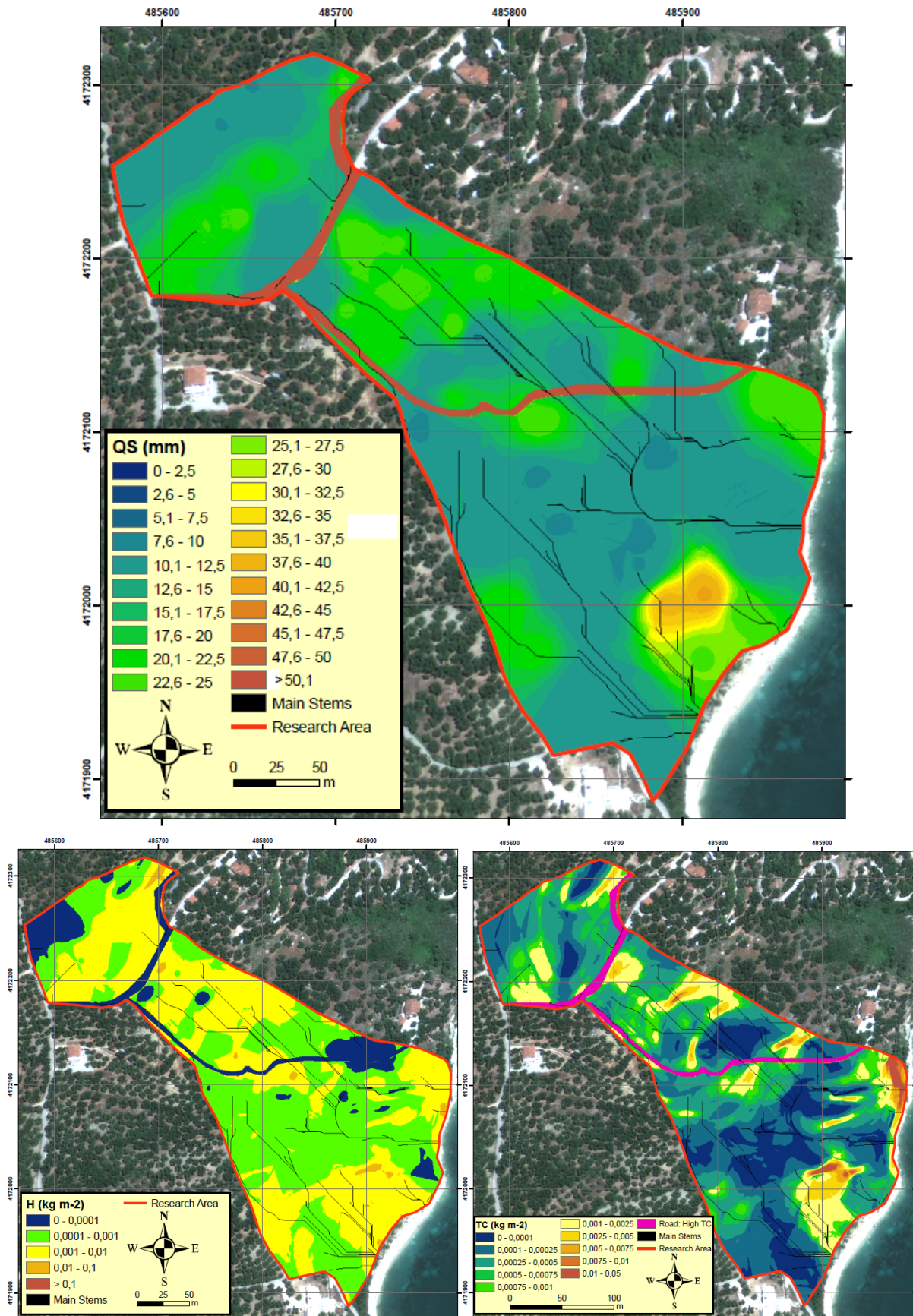


Figure 8: Up: Total annual surface runoff QS (mm); Left below: Detachment by runoff H (kg m<sup>-2</sup>); Right below: Transport capacity TC (kg m<sup>-2</sup>). All estimations are based on the assumption that there are no surface crusts in the area.

In Spata (Greece) Romero-Díaz et al. (1999) took erosion/deposition plot measurements (Wischmeier-Smith type: 10x2m) in semi-natural olive groves where surface sealing was prevented and the velocity of runoff was minimized. Soils mainly existed of sandy loams. The annual runoff per year ranged from 0% to 2.6% of the total rain per year (rainfall amounts varying between 453 and 575 mm) leading to an average runoff of 2 mm. One plot was very similar to the conditions found on Kamaroti. The plot was located on a slope of  $\pm 12^\circ$ , with a clay loam soil, a vegetation cover varying between 44 and 95% and a stone cover of 34%. Runoff values varied between 3.1 and 20.9 mm. This is in the same range as the runoff-estimations made by the MMF-model for Kamaroti.

Runoff estimations correspond also relatively well to values found by Arhonditis et al. (2000) for the Gera watershed (194.01 km<sup>2</sup>) on Lesbos, Greece. Approximately 39% of their study area consisted of cultivated olive groves and 21% of abandoned olive groves. Almost all olive groves (cultivated and abandoned) were terraced. Furthermore land cover types included maquis vegetation (33.2%), wetlands (3.5%) and urban areas (4.4%). The study area has an annual rainfall amount of 600-800 mm. Soils are mainly sandy loams and the average slope is  $\pm 27$  degrees. Runoff measurement values ranged roughly between 30 and 40 mm yr<sup>-1</sup>. This is slightly higher than runoff values estimated for Kamaroti.

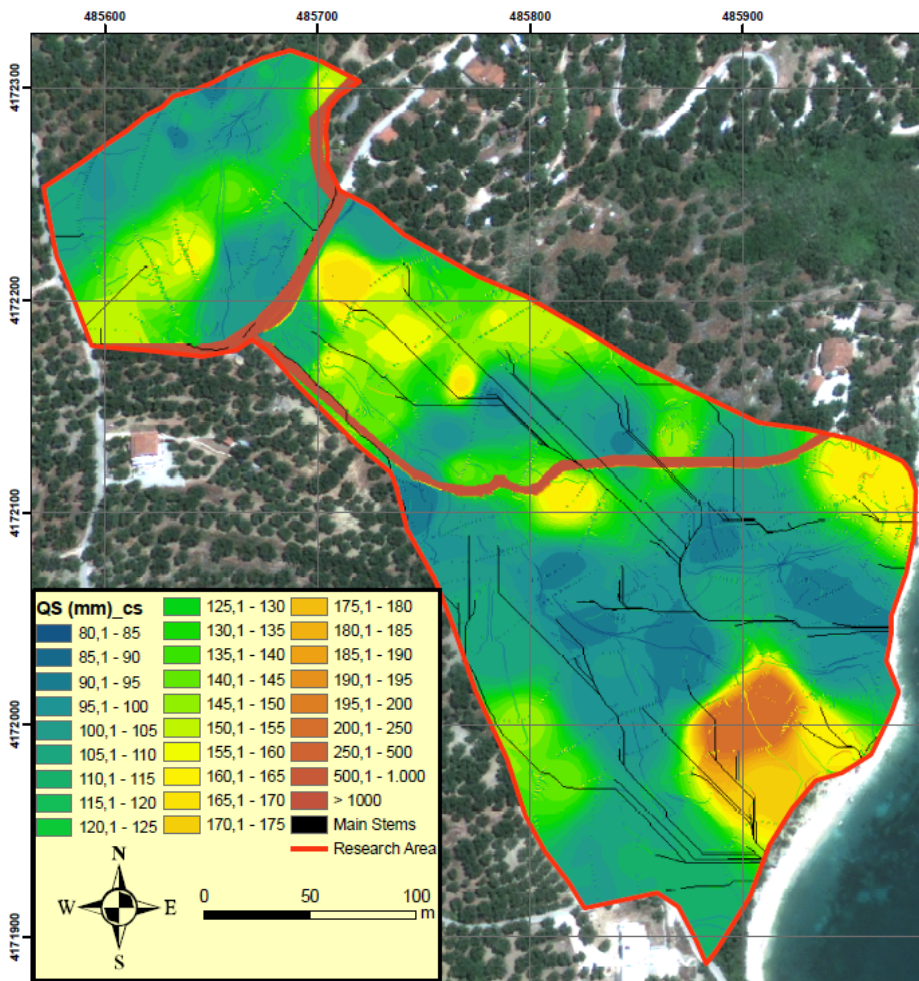


Figure 9: Total annual surface runoff QS (in mm) under surface crust conditions.

With an  $EHD$  of 0.05m (surface crust)  $SC$  has an average of 19.3 mm.  $QR$ -estimations had an average of 105.2 mm for the olive orchards with a standard deviation of 18.9 mm, a minimum of 79.8 mm and a maximum of 173.9 mm.  $QS$  (mm) has an estimated average of 124.8 mm with a standard deviation of 61.5 mm for the orchards (figure 9).  $H$  has an estimated mean of  $0.036 \text{ kg m}^{-2}$  with a standard deviation of  $0.0415 \text{ kg m}^{-2}$ .  $TC$  has an estimated mean of  $0.038 \text{ kg m}^{-2}$  with a standard deviation of  $0.082 \text{ kg m}^{-2}$ .

#### 4.1.3. Soil erosion/deposition

Potential erosion  $E$  is the sum of detachment by runoff  $H$  and detachment by raindrop  $F_{yr}$ .  $E$  plus sediment coming from upstream represents soil available for transport in a raster cell. This is limited by transport capacity  $TC$ . The MMF-model calculates net erosion per raster cell;  $E_{In} - E_{Out}$  (for model design: appendix II). Erosion/deposition estimations for normal conditions provided low quantities of transported soil (figure 10).

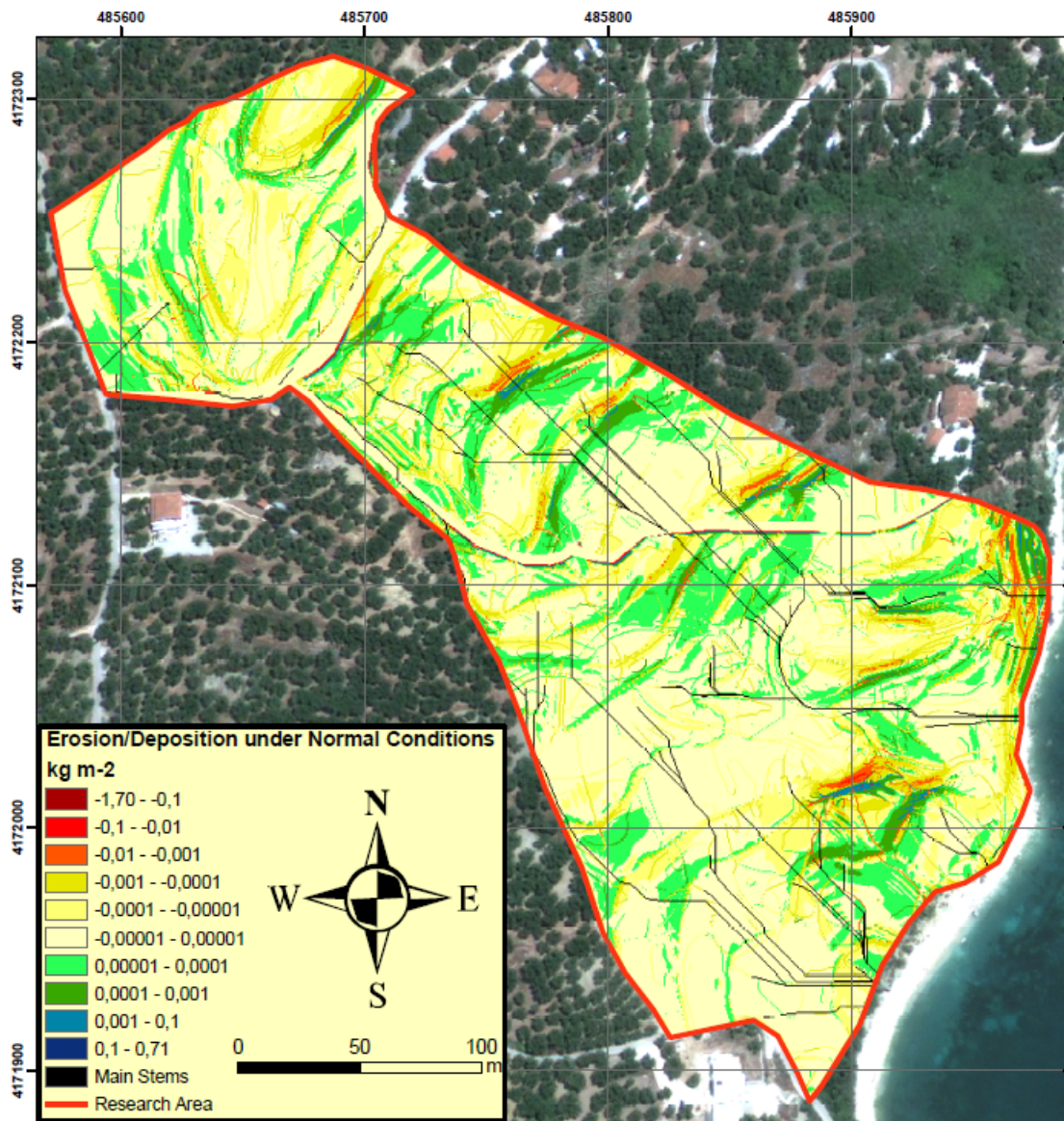


Figure 10: Erosion/deposition  $E_{net}$  ( $\text{kg m}^{-2}$ ) under no surface crust conditions. Erosion is represented by negative values, deposition by positive values.

In the model results erosion occurs in 51.7% of the research area. Raster cells undergoing erosion lose on average  $0.00033 \text{ kg m}^{-2}$  of soil with a standard deviation of  $0.0087 \text{ kg m}^{-2}$ . At this rate a  $\pm 23 \text{ kg}$  of soil is relocated in the entire research area. Approximately 99.5% of the erosive areas lose soil at a lower rate than  $0.01 \text{ kg m}^{-2}$  with a mean erosion rate of  $0.00013 \text{ kg m}^{-2}$  and a standard deviation of  $0.00049 \text{ kg m}^{-2}$ . Erosion rates lower than  $0.001 \text{ kg m}^{-2}$  occur in 98.6% of the research area with a mean erosion rate of  $0.000069 \text{ kg m}^{-2}$  and a standard deviation of  $0.00015 \text{ kg m}^{-2}$ . Erosion rates lower than  $0.0001 \text{ kg m}^{-2}$  occur in 80.0% of the area.

Deposition takes place in 44.6% of the research area. An estimated average of  $0.00021 \text{ kg m}^{-2}$  is deposited per deposition cell. Standard deviation is  $0.0043 \text{ kg m}^{-2}$ . Approximately 99.9% of the depositional areas receive sediment at a lower rate than  $0.01 \text{ kg m}^{-2}$ , 99.7% lower than  $0.001 \text{ kg m}^{-2}$  and 89.4% lower than  $0.0001 \text{ kg m}^{-2}$ . In the areas with lower deposition rates than  $0.001 \text{ kg m}^{-2}$  mean deposition is  $0.00004 \text{ kg m}^{-2}$  with a standard deviation of  $0.00010 \text{ kg m}^{-2}$ .

An estimated 3.7% of the area is considered stable, which means no erosion or deposition takes place. Roads form 94.3% of the stable areas.

No erosion/deposition measurements were done in the field during this research. However, it is possible to compare the estimated amounts to measured values from literature for similar types of areas. Rills and gullies are not taken into account. While rills and gullies are reported to be responsible for 83% of the total soil loss in the Mediterranean (Nachtergaele et al., 2000; Poesen et al., 2002), on Kamaroti just one small gully-like system is present and rills were not observed. It is possible that the absence of rills is a consequence of the timing of the field research. However, unploughed parts of the research area show no signs of rill formation as well. All discussed studies are based on plot measurements.

Model results of the MMF-model seem extremely low in comparison with erosion/deposition measurement values from literature. Geeson et al. (2002) states that degradation of land underneath olive trees, with plant residues and rock cover around 90%, is limited to almost negligible values ( $0.001 \text{ t ha}^{-2}$ ). This value is still 100 times higher than the average model result for Kamaroti. Arhonditsis et al. (2000) measured in the Gera watershed on Lesvos average soil losses of  $0.003 \text{ kg m}^{-2} \text{ yr}^{-1}$  for abandoned olive groves and  $0.0065 \text{ kg m}^{-2} \text{ yr}^{-1}$  for cultivated olive groves. Soil erosion estimations using the PESERA soil erosion model for the Sekania watershed (on Zakynthos) were done by Tsara et al. (2005). Estimations of erosion rates for olive groves range between  $0.003$  and  $0.02 \text{ kg m}^{-2} \text{ yr}^{-1}$ .

The MMF-model probably underestimates erosion/deposition for olive orchards under Mediterranean conditions. This is best represented by MMF-model predictions for Spata (Greece) done by Morgan (2001). While runoff predictions by Morgan were relatively similar to measured runoff values, soil loss predictions show a serious underestimation. Sediment losses were estimated  $0.000 \text{ kg m}^{-2}$  while there was an observed soil loss of  $0.005 \text{ kg m}^{-2}$ . The MMF-runoff estimations for Kamaroti are quite similar to the runoff quantities measured by Romero-Díaz et al. (1999) in Spata under comparable field conditions. Sediment losses were measured 0 to  $0.0028 \text{ kg m}^{-2} \text{ yr}^{-1}$  for the Spata field sites. Sediment yields were  $0.004 \text{ kg m}^{-2} \text{ yr}^{-1}$  for a plot with similar field characteristics as on Kamaroti (Romero-Díaz et al., 1999). This is significantly higher than the soil loss estimations on Kamaroti for normal conditions.

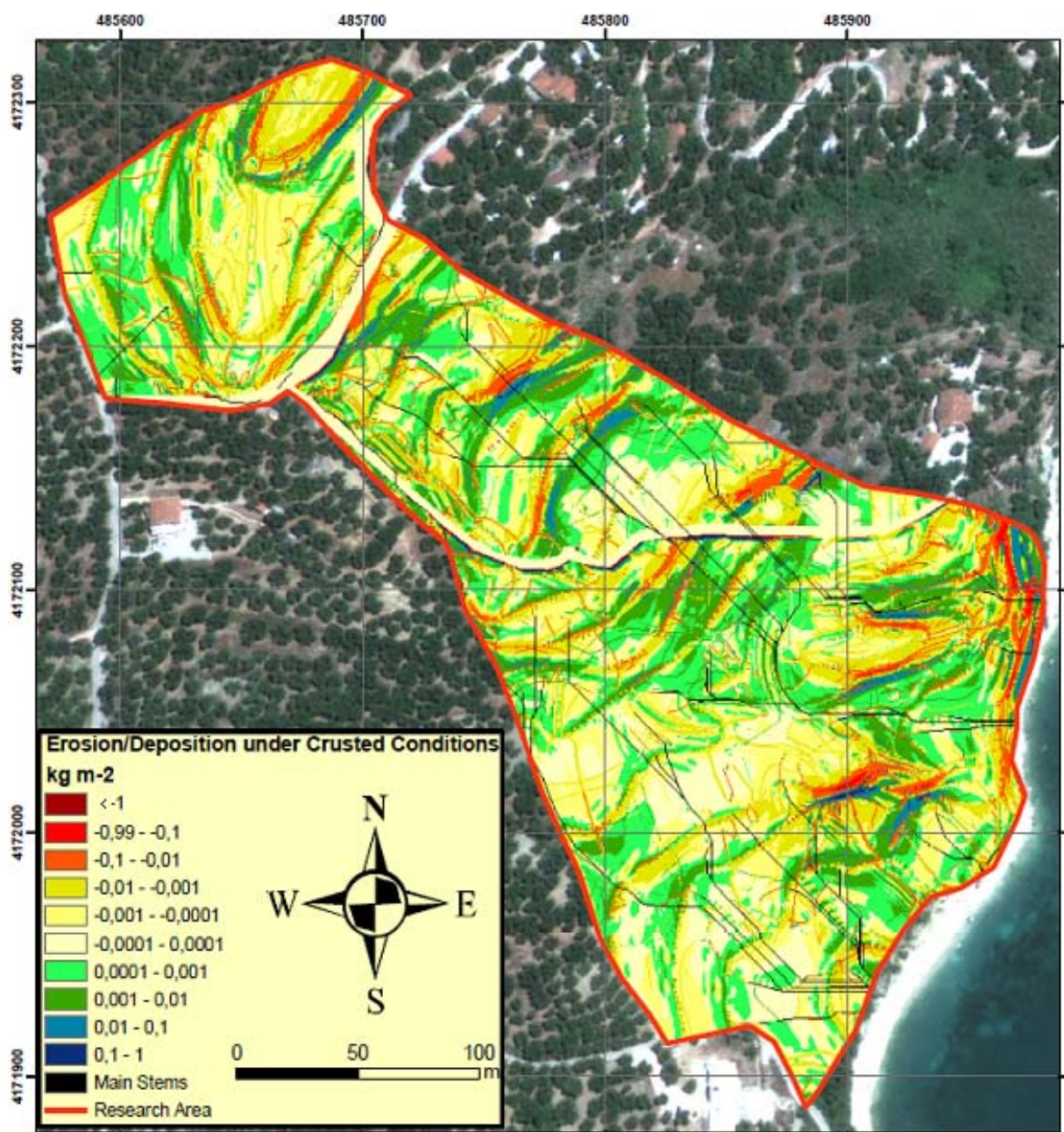


Figure 11: Erosion/deposition  $E_{net}$  ( $\text{kg m}^{-2}$ ) under surface crust conditions. Erosion is represented by negative values, deposition by positive values.

The values found for erosion/deposition under crusted conditions are more similar to values found in literature (figure 11). Eroding areas cover 53.2% of the research area according to the model estimations. Under normal conditions this was estimated at 51.7%. This difference originates in the strong influence of  $QS$  on  $TC$  apropos to the influence of slope  $S$  (equation 16 (§ 3.1)). The stronger increase in runoff along streams compensates for decreasing slope angles, leading to a longer increase in  $TC$  downstream. Mean erosion is  $0.012 \text{ kg m}^{-2}$  with a standard deviation of  $0.170 \text{ kg m}^{-2}$ . Total relocated soil in the entire research area according to these estimations approximates  $821 \text{ kg yr}^{-1}$ . If looked at the raster cells with a smaller soil loss than  $0.1 \text{ kg m}^{-2}$  (98.8% of the eroding areas) mean erosion is  $0.0052 \text{ kg m}^{-2}$  with a standard deviation of  $0.011 \text{ kg m}^{-2}$ . An estimated 84.8% of the area has lower erosion rates than  $0.01 \text{ kg m}^{-2}$  and 52.5% lower than  $0.001 \text{ kg m}^{-2}$ .

Deposition takes place in 43.08% of the research area. Deposition has an average rate of  $0.0078 \text{ kg m}^{-2}$  with a standard deviation of  $0.1088 \text{ kg m}^{-2}$ . Deposition at a lower rate than  $1.0 \text{ kg m}^{-2}$  per year takes place in 99.8% of the research area, 99.2% has a lower rate than  $0.1 \text{ kg m}^{-2}$  and 93.2% lower than  $0.01 \text{ kg m}^{-2}$ . The average deposition in the areas with a lower rate than  $0.1 \text{ kg m}^{-2}$  is  $0.0028 \text{ kg m}^{-2}$  with a standard deviation of  $0.0080 \text{ kg m}^{-2}$ .

There are several areas in the model outputs showing high erosion rates. On the eastern side of the top severe erosion takes place immediately followed by deposition. This was also noted during the field work. The second area of high erosion is just below the road. This is also confirmed by the field observations (figure 12). There are several spots of severe erosion along the hill. These spots are mostly characterized by a rapid increase in slope angle. Depositional areas are characterized by a decrease in slope angle.

The spatial distribution of erosion and deposition predictions (normal and crusted) shows limited transportation of soil. Deposition takes place shortly after particle detachment. This corresponds to field observations made on Kamaroti (figure 12). Soil particles are detached from and deposited at the feet of bare terrace borders. There are no visible signs of transportation across the terraces.

It seems likely that the only way soil can get transported over longer distances in the research area is through gully-like systems. The main stems on the erosion/deposition maps (figure 10 and 11) can be seen as a representation of these gully's. The upkeep of the olive orchards in the research area is especially downhill very limited which means these systems should have a chance to develop. In the field however the geomorphology does not indicate the presence of these systems under summer or winter conditions. Accordingly the choice was made to leave these main stems out of the model estimations.



Figure 12: Top left: Erosion/deposition (485717, 4172184). Top Right: Erosion/deposition below the road (485702, 4172221). The pictures on top are from August 2009.

Below left: Erosion/deposition at terrace border at the western part of the top of Kamaroti (485663, 4172309). Below right: Gully-like system above the road (485673, 4172197). The pictures below are from October 2009.

#### 4.2. Upper part of Kamaroti

A detailed DEM was developed for the upper part of Kamaroti. The goal was to get a precise local drainage pattern. The same steps as for the entire research area were taken to predict erosion/deposition for surface crust and no surface crust conditions.  $F_{yr\_top}$  has a mean of  $1.3 \text{ kg m}^{-2}$  and a standard deviation of  $0.8 \text{ kg m}^{-2}$ .

For no surface crust conditions the runoff from precipitation has an estimated average of 15.1 mm for the olive orchards on the top, with a standard deviation of 4.1 mm (figure 13). On average QS is estimated 14.0 mm, with a standard deviation of 8.1 mm, in the

olive orchards (figure 12). Almost 100% of the olive orchards has a lower  $QS$  than 25 mm and  $\pm 58.8\%$  lower than 15 mm, with a minimum amount of surface runoff of 9.6 mm. Under normal conditions 71.5% of the research area erodes with an average rate of  $0.00046 \text{ kg m}^{-2}$  (standard deviation of  $0.0045 \text{ kg m}^{-2}$ ). Deposition takes place in 21.0% of the area with an average rate of  $0.00029 \text{ kg m}^{-2}$  (standard deviation of  $0.00340 \text{ kg m}^{-2}$ ).

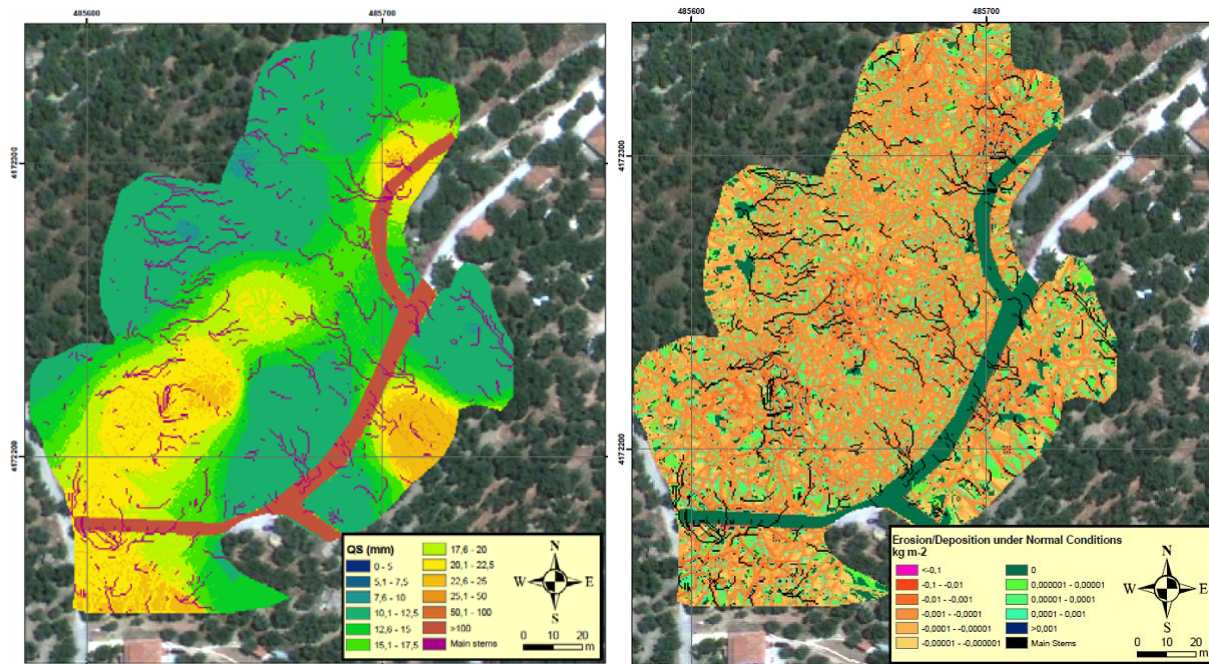


Figure 13: Left: Total surface runoff  $QS$  (mm) for no surface crust conditions. Right: Erosion/Deposition  $E_{net}$  ( $\text{kg m}^{-2}$ ) for no surface crust conditions. Erosion is represented by negative values, deposition by positive values.

For surface crust conditions the runoff from precipitation has an estimated average of 105.6 mm for the olive orchards on the top, with a standard deviation of 14.9 mm (figure 14). Under crusted conditions an average  $QS$  is estimated at 117.8 mm with a standard deviation of 28.5 mm for the olive orchards. Around 88.4% of the olive orchards has a lower estimated  $QS$  than 150 mm and around 24.6% one below 100 mm. The estimated minimum  $QS$  is 76.7 mm.

Erosion takes place in 73.6 % of the research area with a mean annual rate of  $0.025 \text{ kg m}^{-2}$  and a standard deviation of  $0.128 \text{ kg m}^{-2}$ . Deposition occurs in 18.9% of the research area with a mean annual rate of  $0.019 \text{ kg m}^{-2}$  and a standard deviation of  $0.115 \text{ kg m}^{-2}$ .

Similar patterns are seen in comparison to the erosion/deposition estimations of the entire research area. The total area is characterized by a repeated interchange of small eroding and depositional areas. The chaotic pattern of the model outputs is probably provoked by small positive or negative errors of the DGPS-measurements. Although DGPS-points with large errors in elevation were manually adjusted and the *Fill*-function in the Spatial Analyst toolbox in ArcGIS was used to smoothen the DEM, small variations in

height remain. The eroding area on the northeast is also seen in figures 10 and 11, and was noted during the field work. No other specific areas of erosion or deposition can be seen.

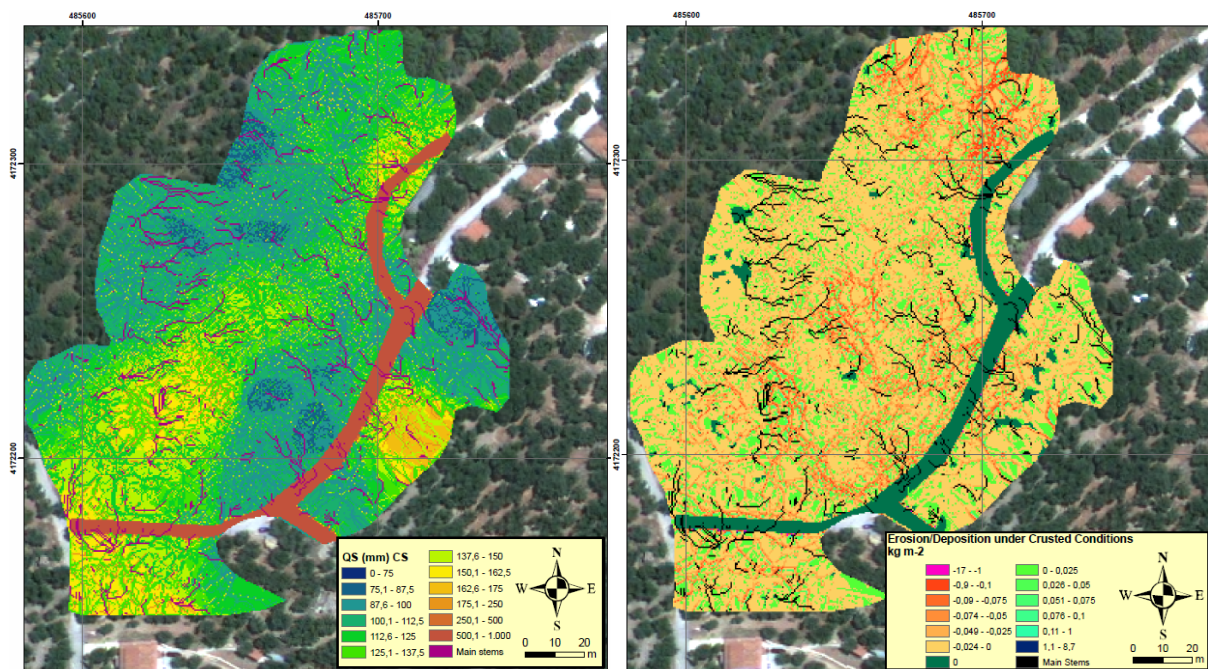


Figure 14: Left: Total surface runoff QS (mm) for surface crust conditions. Right: Erosion/Deposition  $E_{net}$  ( $\text{kg m}^{-2}$ ) for surface crust conditions. Erosion is represented by negative values, deposition by positive values.

### 4.3. Model Uncertainties

The premier idea was to calculate erosion/deposition rates on a monthly basis to preempt the Mediterranean seasonality. This proved to be impossible and therefore the model was applied on a yearly basis. This could lead to overestimation of erosion. During the summer months ground cover is very low which leads to high detachment rates during precipitation events while transportation is limited by the transport capacities of the runoff. If winter transport capacities are more than sufficient the model would see the detachment of particles in summer as relocated soil which would not happen in reality. However, on Kamaroti transport capacities are far lower than detachment of soil particles during the entire year which annuls this possible problem.

An important aspect of the Mediterranean climate in relation to erosion are the incidental torrential rainfall events. Yearly erosion quantities are strongly related to the timing and vehemence of these major erosive events. An extreme precipitation event at the end of summer provokes much higher quantities of erosion than the same event in the middle of the winter months. González-Hidalgo et al. (2007) found that 50% of the soil eroded in a year in the Mediterranean belongs to three daily erosion events. An even higher percentage was found during a study of Dimoyiannis et al. (2006) in Larissa (Greece). During soil erosion measurements in 2001 a one-hour storm event accounted for 64-92%

of the total annual soil loss that year. A similar extreme event on the 29<sup>th</sup> of May 1998, also close to Larissa, was responsible for 41-56 % of total annual runoff (Terzoudi et al., 2007). Another aspect of these major events is the rainfall intensity. The model estimates rainfall intensity  $I$  at an average of  $30 \text{ mm h}^{-1}$ . In central Greece Terzoudi et al. (2007) however measured intensities up to  $70 \text{ mm h}^{-1}$  (for 15 minutes) on the 29<sup>th</sup> of May 1998 and Dimoyiannis et al. (2006) measured up to  $180 \text{ mm h}^{-1}$  (for 5 minutes). These events are far more decisive for the amount of yearly erosion than the total average yearly rainfall in the area. Since such data was unavailable for the research area on Zakynthos the model used average yearly parameters. It does not take the occurrence and timing of these extreme events into account which could lead to underestimation of erosion. The dependence of erosion/deposition quantities on these extreme events makes it difficult to assess the significance of the model results.

Finally input parameters were estimated in the field which can imply misjudgements. Estimations are based on average values of terraces, while microscale differences can have a high impact on erosion/deposition quantities. Examples are the places in the research area with a high stone cover. The patterns of these stone layers can cause significant differences in the erosion/deposition patterns in these areas. Types of terrace borders are not taken into account while they vary highly. Some terrace borders consist of solid terrace walls while some show bare soil with definite erosion/deposition marks. An extra uncertainty in the detailed DEM of the top are high aberrations in the differential GPS measurements. These points had to be manually adjusted to prevent sinks in the DEM. Minor aberrations however were not adjusted, which could lead to important differences in the estimated local drainage patterns and the resulting spatial distribution of eroded soil.

#### **4.4. Model Outputs vs. Artefact Distribution**

The archaeological data was delivered by the Zakynthos Archaeology Project (ZAP) (appendix III). For more information on the ZAP is cited to Van Wijngaarden (2007), Van Wijngaarden et al. (2005) and Van Wijngaarden et al. (2006). The delivered archaeological data is raw, unaltered data and still somewhat vague. The comparison in this thesis between the MMF-model outputs and the artefact distribution is a first interpretation according to the present standing of the archaeological data. Given coordinates correspond to the coordinate system of figure 11 (UTM WGS 84).

The spatial distribution of artefacts was compared with the erosion/deposition map for crusted conditions. Soil crusting was noted during the summer campaign and the predicted erosion/deposition quantities correspond better to values found in literature. Moreover spatial patterns and severity of erosion/deposition are more apparent. A final

argument for using this map is the dependence of yearly soil erosion/deposition on a single, or few, rainfall events in the Mediterranean. Probably most of the transportation of artefacts is related to these extreme rainfall events. Because the MMF-model uses average yearly rainfall quantities as input the timing and vehemence of these events is neglected and thereby their major influence diminished. This leads probably to underestimation of erosion/deposition and therefore the more extreme outputs were used.

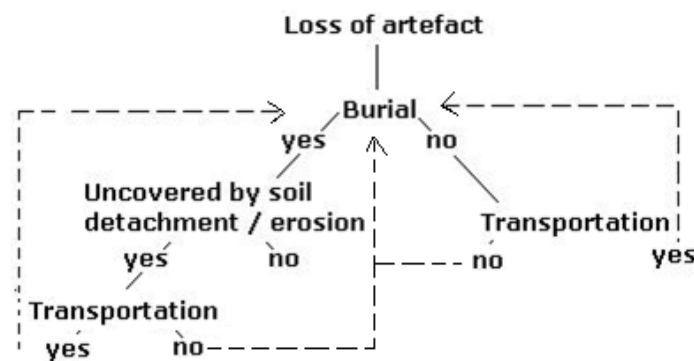


Figure 15: Possible processes determining find location of an artefact.

There are several processes that determine find location and artefact condition (figure 15). An important question is whether artefacts have always been on the surface or if they were uncovered through detachment of soil particles. Artefacts on Kamaroti show different degrees of weathering which is an indication for the time that an artefact has been on the surface. Little is known about artefact weathering rates which means only a qualitative assessment of this time can be given. In the following sections evaluation of the artefact distribution was done by visual comparison of the MMF-model outputs with the archaeological maps. The focus lies on Bronze Age and Ancient material.

### *Upper part of Kamaroti*

Relatively well preserved Bronze Age material was found especially on the north-eastern side of the top area (figure 16). Although all artefacts in this area were picked up during the summer campaign many "new" artefacts were found in October. The speed of surfacing is high which corresponds to the high erosion rates estimated in the model for this area. Field observations show that artefacts surface due to headward erosion in terrace borders (especially in area 1). This eroded material is directly deposited along the terrace borders (figure 12). Artefacts are heavier than soil particles leading to early deposition. It is unlikely that artefacts are transported far away after surfacing.

Ancient/Bronze Age artefact densities are high on the southeastern slope of the top area (area 3). There is a prominent concurrence between high ancient/Bronze Age artefact

densities and high soil particle detachment  $E$  in this area. The artefacts are relatively well preserved and cannot have been on the surface for a long time. It cannot be said with certainty if the artefacts are uncovered here or if they have been transported downwards from the top area. Transportation downwards seems possible since this area is mainly eroding. However, transport capacities are low.

A gully like system is located on the south side of the top of Kamaroti (figure 12; 485673, 4172197). This gully is not present in the model outputs but seems the only possibility of significant transportation of artefacts. Artefacts

are found along the gully and on the road below. These artefacts are relocated from the frontside of area 2. Many artefacts are found on the surface here. Moreover coring (485659, 4172242) revealed a lot of artefacts in the subsurface of this area.

On the western side of the area Venetian-recent material is found (area 4). Artefact densities are low. This is mainly a depositional area. No ancient artefacts are transported down from the top area, mainly because deposition takes place shortly after erosion. Stream powers are probably too low to transport the artefacts over the large bench terraces. An important feature in this area is an ancient road (485600, 4172230) where high quantities of Bronze Age material were found. This material is probably in situ which means transportation of artefacts in general must be limited. This is supported by the low estimations of erosion/deposition.

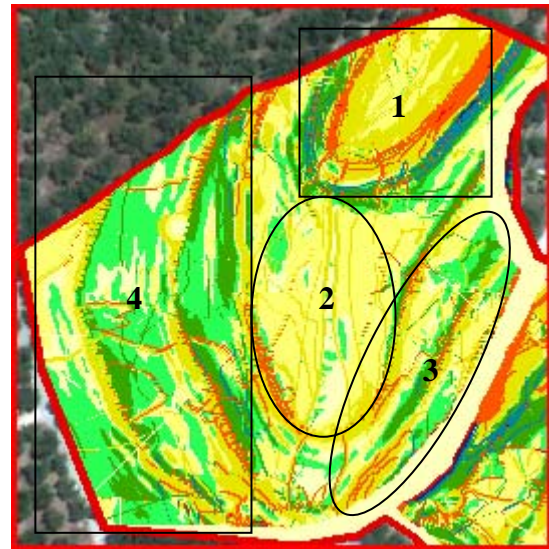


Figure 16: Estimated erosion/deposition under crusted conditions on the top of Kamaroti. For legend see figure 11.

### *Middle Part of Kamaroti*

Severe erosion takes place directly underneath the road (figure 12; figure 17 (area 5)). No ancient artefacts surface here. Artefact densities are very low in area 5 (0.001-0.004 ancient artefacts/m<sup>2</sup>). The material found is heavily weathered indicating a prolonged stay on the surface. Nowadays (almost) no water can come into this area from the top. Ancient artefacts must have been transported here long ago or were lost in this area. Modern erosion/deposition seems of no significant influence.

Area 6 shows quick alterations of eroding and depositional areas. No data on the archaeological material of this area is present.

High artefact quantities are found in area 7. Bronze Age and Early Iron Age material was found here. The artefacts are much worn meaning a prolonged stay on the surface. It seems impossible that these artefacts have been transported here through modern

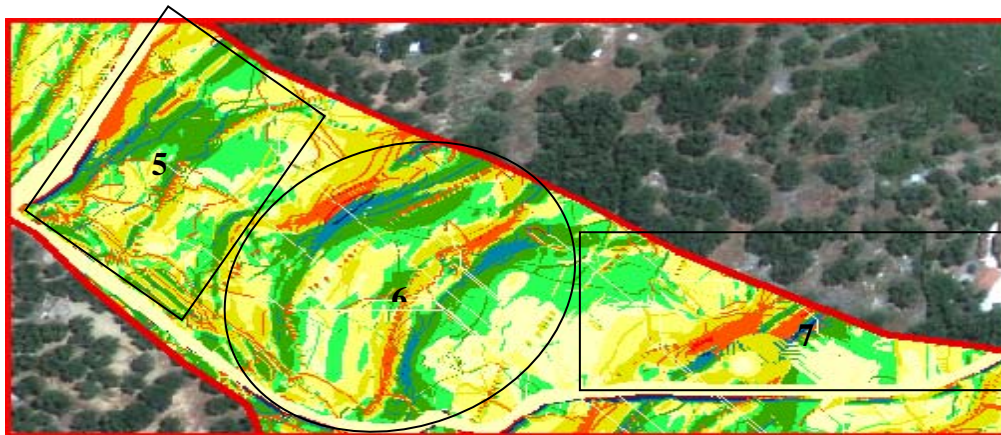


Figure 17: Estimated erosion/ deposition under crusted conditions on the middle part of Kamaroti. For legend see figure 11.

erosion/deposition. Erosion/deposition rates in the upstream area seem too low. Furthermore no indications are found in the field of rills or gully-like systems which can transport artefact over long distances. The quick alterations in erosion/deposition make sure that if artefacts are detached they deposit quickly.

#### Lower Part of Kamaroti

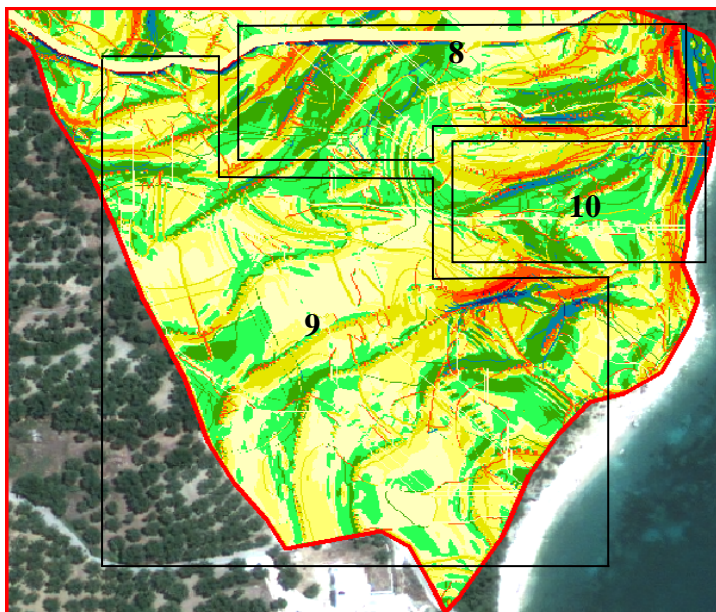


Figure 18: Estimated erosion/deposition under crusted conditions on the lower part of Kamaroti. For legend see figure 11.

In the western part of area 8 (figure 18) mainly Venetian-recent material was found. Further to the east high quantities of severely weathered Ancient/Bronze Age material were found. In this area two pieces of the same pithos (vase) were found. It seems unlikely that two pieces are relocated together. Area 8 is nowadays estimated to be an area of slow deposition.

A largely stable area with low quantities of Venetian-Recent material can be found in the south of the research area (area 9). It is estimated that almost no transportation of soil takes place here.

Area 10 is surrounded by large rocks. No soil can enter here from above. Many, relatively well preserved, Ancient/Bronze Age artefacts were found here. These artefacts must lie in

situ. The erosion/deposition estimations show spots of high erosion surrounding this area. These spots are solid rock and represent a small error in the model estimations.

*Entire research area*

In general modern erosion/deposition seems insignificant to the artefact distribution. The quick alteration of erosion/deposition and low transport capacities make sure that artefacts undergo no significant transportation. More artefacts were found on eroding than on depositional areas (figure 19), but the difference seems of no significance. Furthermore there is no apparent relation between artefact distribution and particle detachment  $E$ . The correlation matrix shows a correlation of -0.059 between total particle detachment  $E$  and the amount of artefacts/m<sup>2</sup>. For areas with more than 0.01 artefact/m<sup>2</sup> the correlation is 0.062. The area southeast of the top were high artefact densities correspond to high particle detachment  $E$  seems coincidence. Moreover the majority of the artefacts found on Kamaroti are heavily weathered. This indicates a prolonged stay at the surface.

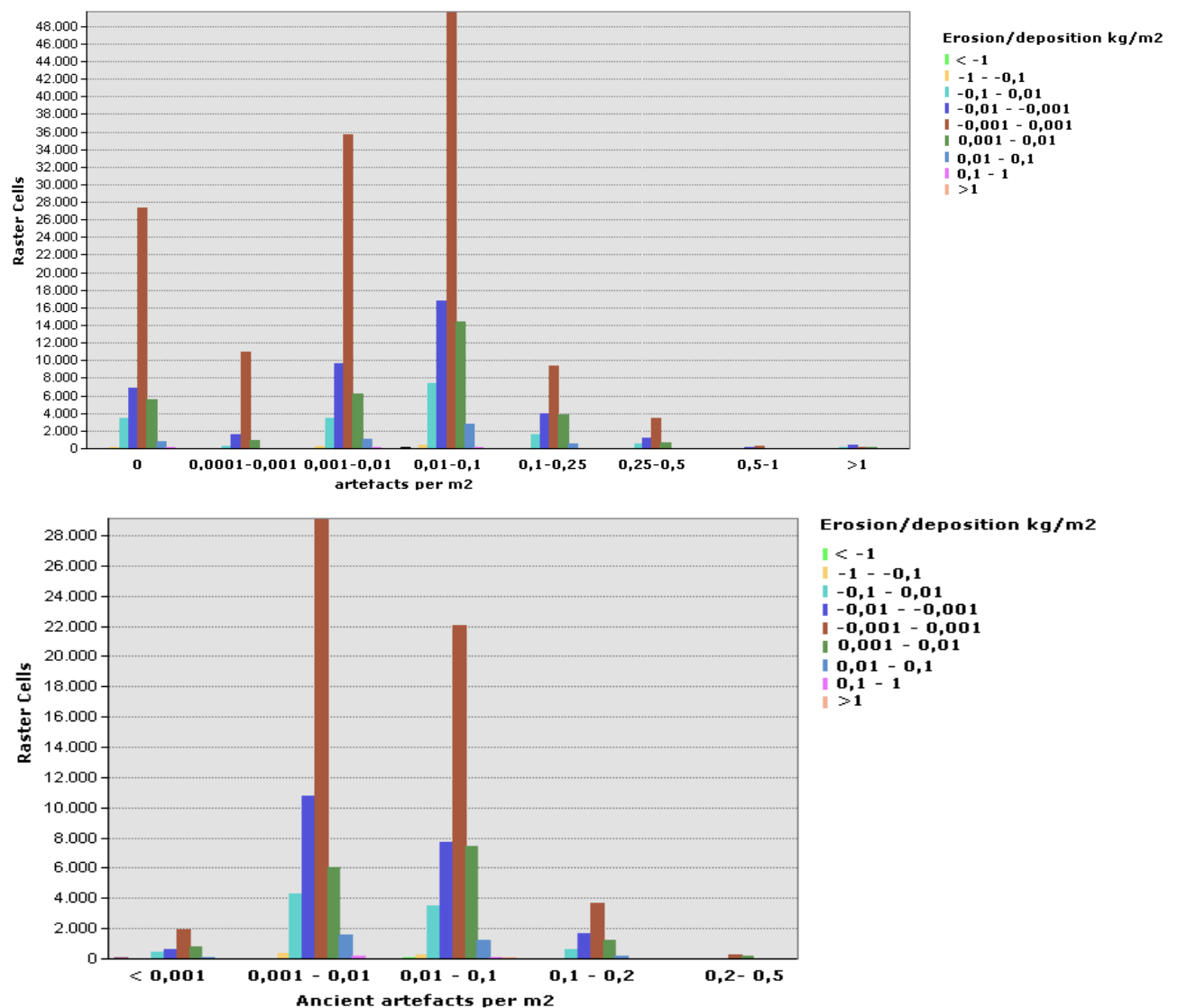


Figure 19: Above: Erosion/deposition vs. artefacts/m<sup>2</sup>. Below: Erosion/deposition vs. ancient artefacts/m<sup>2</sup>.

### 5. Historic Soil Erosion vs. Artefact Distribution

Modern erosion/deposition, apart from uncovering artefacts, has little influence on the spatial pattern of archaeological material. But perhaps historical erosion/deposition is of importance? The focus lies on the period from the start of the Bronze Age, 5 cal kyr BP, until present. The geomorphologic evolution of the research area was investigated through the subsurface stratigraphy by Bekkers (2010).

Climatic circumstances in the Mediterranean during the Bronze Age were almost similar to the present climate. Average year, summer and winter temperatures were a little colder than nowadays. Yearly precipitation values were slightly higher, especially during the summer period (Dormoy et al., 2009; Bar-Matthews et al., 2003). Vegetation consisted of mixed forests, with mainly *Quercus*, *Carpinus orientalis* and *Ostrya*. At 5.5 cal kyr BP there is a slight increase in *Olea* to 1-2% in the pollen records of the Mediterranean. *Phillyrea* values increase, indicative for Mediterranean conditions, as well as the values of evergreen oaks. An increased dominance of *Phillyrea* (up to 40% of the pollen record in Lake Voulkaria; a coastal lake 150 km north of Zakynthos) at the expense of boreal pollen is assumed to indicate the start of a dry period in the Mediterranean from 2.8 cal kyr BP on. At 2.7 cal kyr BP however values of deciduous oaks increased again around Lake Voulkouria. Furthermore human development becomes more visible with increasing *Olea* and *Juglans* (Jahns, 2005). The last phase reveals a decrease in *Pistacia* while *Fraxinus angustifolia* increased. A renewed increase in *Olea* at the expense of deciduous oaks took place. The large degree of woodland clearance and agricultural development of modern time is not reflected in the pollen record around Lake Voulkouria. The scarcity of trees in the modern environment is suggested to be relatively recent. A pollen diagram of Lake Ozeros in central Acarnania shows that further inland areas were densely wooded until at least 1.0 cal kyr BP (Jahns, 2005).

The changes in climate in the middle-Mediterranean over the last 5000 years seem not so drastic. It is possible that vegetation changes have altered erosion/deposition patterns and quantities on Kamaroti. Alteration of topology by means of uplift and ongoing seismic activity in the area could be of much higher influence on erosion/deposition and the artefact distributions in the area. An uplift of 43.10 mm, with a root mean square error of 8.2 mm, was measured with DGPS in the area between August 2005 and July 2006 (Lagios, 2007). It is unlikely that this uplift has been stable over the last 5000 years. However, Kamaroti was probably somewhat lower and less steep in ancient times.

A radical alteration in the area took place between 1986-1993. Bulldozered terracing must have altered the outlook and hydrology on Kamaroti significantly (Van Wijngaarden, 2009). Erosion was probably higher before the terracing because it reduced runoff

transport capacities along the terraces. Transportation of soil must have been possible between the top and the lower areas on the southwest. It seems likely that because of the cut-off to form terraces layers with archaeological material were breached. The surfacing of archaeological material happens on a much higher rate along the bare terrace walls than before the terracing. This is supported by the pace and the amount of artefacts surfacing along terrace borders and the relatively well preserved artefacts found around the top area.

Only in the middle part of the research area no bulldozered terracing took place. The area has not been altered much (figure 18 (8 and 10)). This area is probably not representative for the rest of Kamaroti before the bulldozering took place. It is considerably rockier and soils are much shallower than in the rest of the research area. Bedrock depths vary highly along the research area. Bedrock depths are lowest in the middle-east of the research area. In the western parts and on the top of Kamaroti soils are at least two meters deep. The high artefact densities in the middle-east of the area (figure 17 (7); figure 18 (8)) correspond to the area where soils are shallow. The artefacts here are considerably worn. It is possible that during ancient times extreme rainfall events generated the stream power needed to transport artefacts downwards. Since artefacts are faster deposited than soil particles they settled quickly while soil particles remained in suspension. In this area however multiple pieces of the same pithos were found in the same tract. Therefore it is more likely that extreme events removed soil in this area while leaving artefacts unmoved. Maybe even because of human occupation soils here were exposed to erosion, leading to much shallower soils in comparison with the upslope area.

An option for future research is to relate stream powers generated by, for example, 500 yr precipitation events in the area to the stream powers needed to transport artefacts of different sizes. Stream powers needed to transport artefacts can possibly be derived from literature data on stream powers needed to transport gravel. By relating transport capacities of these extreme events to the local drainage pattern before the terracing, by usage of the topographical map of 1970, the possible link between the high artefact density areas on the top and in the middle part could be further investigated. Considering the present knowledge of erosion/deposition and the artefact densities it seems likely that artefacts have not been transported from the top downwards. It is probable that the high rate of surfacing of artefacts on the top started after the bulldozered terracing of the area. The artefacts in the middle part are highly weathered and must have been on the surface for a long time. The shallow soils in this area suggest removal of soil rather than addition of artefacts from upslope. This could be explained by exposure of the soil to erosion due to vegetation removal by human settlement in this area.

### **6. Conclusion**

Modern soil erosion/deposition seems of no importance to the archaeological artefact distribution in the entire research area. Continued headward erosion into bare terrace borders brings artefacts to the surface. This process has probably started after the bulldozered terracing of the top area. The drop in transport capacity at the lower part of the terrace borders makes sure deposition takes place almost directly after detachment. This is supported by the observations made in the field. Some transportation took place along a gully-like system in the upper part of the research area. This system is located at the southside of the upper part of Kamaroti, above the road. However, these systems are no part of the model. Furthermore, there is nowadays no transportation further downwards.

It seems unlikely that transportation of artefacts from the upper part to the middle part of Kamaroti has taken place. In one tract two pieces of the same pithos were found which makes transportation from upslope unlikely. The soil in the middle part is very shallow. It seems likely that the soil has been eroded away through time while artefacts remained at the surface. This could explain why the artefacts are heavily weathered. Exposure of the soil to erosion due to vegetation removal by human settlement could be the reason for this locally eroded area. The deep soils upslope of this area indicate little soil erosion and probably a high vegetation cover throughout (human) history.

Erosion/deposition modelling to evaluate artefact assemblies seems a good option in areas where stream powers are high enough to transport artefacts. An option for future research is to relate stream powers generated by, for example, 500 yr precipitation events in an area to the stream powers needed to transport artefacts of different sizes. Stream powers needed to transport artefacts can possibly be derived from literature data on stream powers needed to transport gravel. By relating transport capacities of these extreme events to the local drainage pattern a faster and more precise way of relating artefact assemblies to erosion/deposition could be found. Especially in the Mediterranean area where a high percentage of the total relocated soil per year belongs to a few high precipitation events.

### Literature

- Abu Hammad, A., Lundekvam, H., Børresen, T., 2005. *Adaptation of RUSLE in the Eastern Part of the Mediterranean Region*. Earth and Environmental Science 34, 6, 829-841.
- Arhonditsis, G., Giourga, C., Lournou, A., 2000. *Ecological patterns and comparative nutrient dynamics of natural and agricultural Mediterranean-type ecosystems*. Environmental Management 26, 5, 527-537.
- Arhonditsis, G., Giourga, C., Lournou, A., Koulouri, M., 2002. *Quantitative assesment of agricultural runoff and soil erosion using mathematical modeling : Applications in the Mediterranean region*. Environmental Management 30, 3, 434-453.
- Ariztegui, D., Asioli, A., Lowe, J.J., Trincarde, F., Vigliotti, L., Tamburini, F., Chondrogianni, C., Accorsi, C.A., Bandini Mazzanti, M., Mercuri, A.M., Van der Kaars, S., McKenzie, J.A., Oldfield, F., 2000. *Paleoclimate and the formation of sapropel S1: inference from Late Quaternary lacustrine and marine sequences in the central Mediterranean region*. Palaeogeography, Palaeoclimatology, Palaeoecology 158, 215-240.
- Avramidis, P., Kontopoulos, N., 2009. *Holocene evolution and sedimentation of Alikes Lagoon, Zakynthos Island, Western Greece: preliminary results*. eEarth 4, 23-29.
- Badia, B., Marti, C., 2008. *Fire and rainfall energy effects on soil erosion and runoff generation in semi-arid forested lands*. Arid land and research management 22, 93 – 108.
- Bar-Matthews, M., Ayalon, A., Gilmour, M., Matthews, A., Hawkesworth, C.J., 2003; *Sea-land oxygen isotopic relationships from planktonic foraminifera and speleotherms in the Eastern Mediterranean region and their implication for paleorainfall during interglacial intervals*. Geochimica et Cosmochimica Acta 67, 17, 3181 – 3199.
- Bekkers, M.N., 2010. *Geomorphological development of Zakynthos, Greece: Relating geomorphology and artefact distribution*. Msc Research Physical Geography, Utrecht University.
- Berendsen, H.J.A., Stouthamer, E., 2001. *Paleogeographic development of the Rhine-Meuse delta-The Netherlands*. Assen: Van Gorcum, eerste druk, 268 p.
- Bintliff, J., 2002. *Time, process and catastrophism in the study of Mediterranean alluvia I history: a review*. World Archaeology 33, 3, Ancien Ecodisasters, 417-435.
- Deng, Z., de Lima, J.L.M.P., Jung, H., 2008. *Sediment transport rate-based model for rainfall induced soil erosion*. Catena 76, 54-62.
- Diamantopoulou, P., Voudouris, K., 2007. *Optimization of water resources management using SWOT analysis: the case of Zakynthos Island, Ionian Sea, Greece*. Environmental Geology 54, 197-211.
- Diodato, N., 2004. *Estimating RUSLE's rainfall factor in the part of Italy with a Mediterranean rainfall regime*. Hydrology and Earth System Sciences 8 (1), 103-107.
- Dimoyiannis, D., Valmis, S., Danalatos, N.G., 2006. *Interrill erosion on cultivated Greek soils: modelling sediment delivery*. Earth Surface Processes and Landforms 31, 940-949.
- Dormoy, I., Peyron, O., Combourieu Nebout, N., Goring, S., Kotthoff, U., Magny, M., Pross, J., 2009. *Terrestrial climate variability and seasonality changes in the Mediterranean region between 15000 and 4000 years BP deduced from marine pollen records*. Climate of the Past, 615-632.
- Favaretto, S., Asioli, A., Miola, A., Piva, A., 2008. *Preboreal climatic oscillations recorded by pollen and foraminifera in the southern Adriatic Sea*. Quaternary International 190, 89-102.
- Fifield, J., 1995, *Practical Approaches for Effective Erosion & Sediment Control - A Short Course*, International Erosion Control Association, Steamboat Springs, CO.

- Fuchs, M., Lang, A., Wagner, G.A., 2004. *The history of Holocene soil erosion in the Phlious Basin, NE Peloponnese, Greece, based on optical dating*. *Holocene*, 14 (3), 334-345.
- Fuchs, M., 2007. *An assessment of human versus climatic impacts on Holocene soil erosion in NE Peloponnese, Greece*. *Quaternary research* 67, 349-356.
- Geeson, N.A., Brandt, C.J., Thornes, J.B., 2002. *Mediterranean desertification; A mosaic of processes and responses*. John Wiley & Sons Ltd, Chichester.
- Ghazavi, G., Thomas, Z., Hamon, Y., Marie, J.C., Corson, M., Merot, P., 2008. *Hedgerow impacts on soil-water transfer due to rainfall interception and root-water uptake*. *Hydrological Processes*, 22, 4723-4735.
- Gómez, J.A., Giráldez, J.V., Fereres, E., 2001. *Rainfall interception by olive trees in relation to leaf area*. *Agricultural Water Management* 49, 65-76.
- Gómez, J.A., Sobrinho, T.A., Giráldez, J.V., Fereres, E., 2009. *Soil management effects on runoff, erosion and soil properties in an olive grove of Southern Spain*. *Soil & Tillage Research* 102, 5-13.
- González-Hidalgo, J.C., Peña-Monné, J.L., de Luis, M., 2007. *A review of daily soil erosion in Western Mediterranean areas*. *Catena* 71, 193-199.
- Gournelos T., Evelpidou N. and Vassilopoulos A., 1999. A morphometric analysis using GIS to deduce geomorphological process – natural hazards, at Zakynthos island. *Proceedings of the 6th international conference on Environmental Science and Technology*, Samos, volume II, 371-378.
- Hasiotis, T., Papatheodorou, G., Ferentinos, G., 2005. *A high resolution approach in the recent sedimentation processes at the head of Zakynthos Canyon, western Greece*. *Marine Geology* 214, 49-73.
- Hughes, P.D., Gibbard, P.L., Woodward, J.C., 2007. *Geological controls on Pleistocene glaciation and cirque form in Greece*. *Geomorphology* 88, 242-253.
- James, P.A., Mee, C.B., Taylor, G.J., 1994. *Soil Erosion and the Archaeological Landscape of Methana, Greece*. *Journal of Field Archaeology* 21(4), 395-416.
- Jahns, S., 2005. *The Holocene history of vegetation and settlement at the coastal site of Lake Voulkaria in Arcarnania, western Greece*. *Vegetational History Archaeobot* 14, 55-66.
- Kati, M., Scholle, P.A., 2008. *The Porosity Evolution of Eocene Limestones in the Preapulian Zone, Zakynthos Island, Western Greece*. *Search and Discovery*, Article #50060.
- Kirby, M.J., 1976. *Hydrological slope models: the influence of climate*. In: Derbyshire, E. (Ed.), *Geomorphology and Climate*. Wiley, London, 247-267.
- Konert, M., Vandenberghe, J., 1997. *Comparison of laser grain size analysis with pipette and sieve analysis: a solution for the underestimation of the clay fraction*. *Sedimentology* 44, 523-535.
- Kouli, M., Soupios, P., Vallianatos, F., 2008. *Soil erosion prediction using the Revised Universal Soil Loss Equation (RUSLE) in a GIS framework, Chania, Northwestern Crete, Greece*. *Environmental Geology* 57, 483-497.
- Lagios, E., Sakkas, V., Papadimitriou, P., Parcharidis, I., Diamata, B.N., Chousianitis, K., Vassilopoulou, 2007. *Crustal deformation in the Central Ionian Islands (Greece): Results from DGPS and DInSAR analyses (1995-2006)*. *Tectonophysics* 444, 119-145.
- Lawson, I., Frogley, M., Bryant, C., Preece, R., Tzedakis, P., 2004. *The Lateglacial and Holocene environmental history of the Ioannina basin, north-west Greece*. *Quaternary Science Reviews* 23, 1599-1625.
- Lekkas, E., 1993. *Neotectonic map of Greece, Zakynthos –Volime, scale 1:50000*. University of Athens, 116 p.

- Lo, A., El-Swaify, S.A., Dangler, E.W., Shinshiro, L., 1985. *Effectiveness of  $EI_{30}$  as an erosivity index in Hawaii*. Soil erosion and conservation society of America, Ankeny, 384-392.
- Lopez-Vicente, M., Navas, A., 2005. *Predicting Soil Erosion With RUSLE in Mediterranean Agricultural Systems at Catchment Scale*. Department of Soil and Water, Zaragoza.
- Lopez-Vicente, M., Navas, A., Machin, J., 2008. *Modelling Soil Detachment Rates in Rainfed Agrosystems in South-Central Pyrenees*. Agricultural Water Management 95, 1079-1089.
- Marchal, O., Cacho, I., Stocker, T.F., Grimalt, J.O., Calvo, E., Marstrat, B., Shackleton, N., Vautravers, M., Cortijo, E., Van krevelde, S., Andersson, C., Koc, N., Chapman, M., Scaffi, L., Duplessy, J. C., Sarthein, M., Turon, J.L., duprat, J., Jansen, E., 2002. *Apparent long-term cooling of the sea surface in the northeast Atlantic and the Mediterranean during the Holocene*. Quaternary Sciences Review 21, 455-483.
- Margari, V., Gibbard, P.L., Bryant, C.L., Tzedakis, P.C., 2009. *Character of vegetational and environmental changes in southern Europe during the last glacial period: evidence from Lesbos Island, Greece*. Quaternary Science Reviews 28, 1317-1339.
- Martinez, J.R.F., Durán Zuazo, V.H.D., Raya, A.M., 2006. *Environmental impact from mountainous olive orchards under soil management systems (SE Spain)*. Science of the Total Environment 358, 46-60.
- Mitasova, H., Hofierka, J., Zlocha, M., Iverson, L.R., 1996. *Modelling topographic potential for erosion and deposition using GIS*. International journal of geographic information science 10, 629-641.
- Morgan, R.P.C., 2001. *A simple approach to soil loss prediction: a revised Morgan–Morgan–Finney model*. Catena 44, 305–322.
- Morgan, R.P.C., Morgan, D.D.V., Finney, H.J., 1984. *A predictive model for the assessment of erosion risk*. Journal of Agricultural Engineering Research 30, 245-253.
- Morgan, R.P.C., Duzant, J.H., 2008. *Modified MMF (Morgan-Morgan-Finney) model for evaluating effects of crops and vegetation cover on soil erosion*. Earth Surface Processes and Landforms 32, 90-106.
- Mutua, B.M., Klik, A., Loiskandl, W., 2006. *Modelling soil erosion and sediment yield at a catchment scale: the case of Masinga catchment, Kenya*. Land degradation & development 17, 557-570.
- Nachtergaele, J., Poesen, J., Vandekerckove, L., Oostwoud, D., Roxo, M., 2000. *Testing the ephemeral gully erosion model (EGEM) for two Mediterranean environments*. Earth Surface Processes and Landforms 26, 17-30.
- Papazachos, B., Papazachou, C., 1997. *The Earthquakes of Greece*. Ziti Publications, Thessaloniki, Greece, 304 p.
- Pfeffer, K., 2003. *Intergrating spatio-temporal environmental models for planning ski runs*. PhD research Utrecht University, Netherlands Geographical Studies 311.
- Pnevmatikos, J.D., Katsoulis, B.D., 2006. *The changing rainfall regime in Greece and its impact on climatological means*. Meteorological Applications 13, 331-345.
- Poesen, J., Vandekerckhove, L., Nachtergaele, J., Oostwoud Wijdenes, D., Verstraeten, G., van Wesemael, B., 2002. *Gully erosion in dryland environments*. In: bull, L.J., Kirkby, M.J. (Eds.). *Dryland Rivers: Hydrology and geomorphology of semi-arid channels*. John Wiley and sons, Chichester, 229-262.
- Renssen, H., Isarin, R.F.B., Jacob, D., Podzun, R., Vandenberghe, J., 2001. *Simulation of the Younger Dryas climate in Europe using a regional climate model nested in an AGCM: preliminary results*. Global and Planetary Change 30, 41-57.

- Ripley, J.L., 1998. *A geoarchaeological approach to using surface sites for paleoenvironmental reconstructions*. *Geoarchaeology* 13(8), 793-818.
- Romero-Diaz, A., Cammeraat, L.H., Vacca, A., Kosmas, C., 1999. *Soil erosion at three experimental sites in the Mediterranean*. *Earth Surface Processes and Landforms* 24, 1243-1256.
- Saavedra, C., 2005. *Estimating spatial patterns of erosion and deposition of the Andean region using geo-information techniques. A case study in Cochabamba, Bolivia*. ITC dissertation 128.
- Shreve, R.L., 1967. *Infinite Topologically Random Channel Networks*. *Journal of Geology* 75, 178-186.
- Svorin, J., 2003. *A test of three soil erosion models incorporated into a geographical information system*. *Hydrological Processes* 17, 967-977.
- Tartaron, T.F., Gregory, T.E., Pullen, D.J., Noller, J.S., Rothaus, R.M., Rife, J.L., Tzortzopoulou-Gregory, L., Schon, R., Caraher, W.R., Pettegrew, D.K., Nakassis, D., 2006. *The Eastern Korinthia Archeological Survey- Integrated methods for a dynamic landscape*. *Hesperia* 75 (4), 453-523.
- Terzoudi, C.B., Gemtos, T.A., Danalatos, N.G., Argyrokastritis, 2007. *Applicability of an empirical runoff estimation method in central Greece*. *Soil and Tillage Research* 92, 198-212.
- Theodoros, G., Vassilopoulos, A., Niki, E., 1997. *Development of a GIS - Based methodology to analyze geological, geomorphological and environmental data of the island of Zakynthos*.
- Tsara, M., Kosmas, C., Kirkby, M.J., Kosma, D., Yassoglou, N., 2005. *An evaluation of the PESERA soil erosion model and its application to a case study in Zakynthos, Greece*. *Soil Use and Management* 21, 377-385.
- Van Leeuwen, W.J.D., Sammons, G., 2004. *Vegetation dynamics and soil erosion modeling using remotely sensed data (MODIS) and GIS*. Tenth Biennial USDA Forest Service Remote Sensing Applications Conference, 5-9 April 2004, Salt Lake City, UT.
- Van Walleggem, T., Laguna, A., Giráldez, J.V., Jiménez-Hornero, F.J., 2010. *Applying a simple methodology to assess historical soil erosion in olive orchards*. *Geomorphology* 114, 294-302.
- Van Wijngaarden, G.J.M., 2007. *Zakynthos Archaeology Project 2007 - Summery Report*.
- Van Wijngaarden, G.J.M., 2009. *Zakynthos Archaeology Project 2009 - Summary Report*.
- Van Wijngaarden, G.J.M., Arapogianni, X., Rink, R., Tourloukis, V., 2005. *The Zakynthos survey 2005 - Preliminary report of a pilot survey*. *Pharos, Journal of the Netherlands Institute in Athens* 13, 59-76.
- Van Wijngaarden, G.J.M., Sotiriou, A., Pieters, N., Tourloukis, V., 2006. *The Zakynthos Archaeology Project 2006 - Preliminary report of the first season*. *Pharos, Journal of the Netherlands Institute in Athens*.
- Vrieling, A., De Jong, S.M., Sterk, G., Rodrigues, S.C., 2008. *Timing of erosion and satellite data: A multi-resolution approach to soil erosion risk mapping*. *International Journal of Applied Earth Observation and Geoinformation* 10, 267-281.
- Waters, M.R., 2000. *Alluvial stratigraphy and geoarchaeology in the American Southwest*. *Geoarchaeology* 15(6), 537-557.
- Wells, L., 2001. *A geomorphological approach to reconstructing archaeological settlement patterns based on surficial artefact distribution*. *Earth Sciences and Archaeology*. Kluwer Academic/Plenum Publishers, 107-142.
- Wilson, G.P., Reed, J.M., Lawson, I.T., Frogley, M.R., Preece, R.C., Tzedakis, P.C., 2008. *Diatom response to the Last Glacial-Interglacial Transition in the Ioannina basin, northwest Greece: implications for Mediterranean Palaeoclimate reconstruction*. *Quaternary Science Reviews* 27, 428-440.

Wischmeijer, W.H., Smith D.D., 1978. *Predicting rainfall erosion losses*. Agricultural Handbook 537. USDA. Agricultural Research Service, Washington DC.

Yue-Qing, X., Xiao-Mei, S., Xiang-Bin, K., Jian, P., Yun-Long, C., 2008. *Adapting the RUSLE and GIS to model soil erosion risk in a mountains karst watershed, Guizhou Province, China*. Earth and Environmental Science 141 (1-3), 275-286.

Zachar, D., 1982. *Soil Erosion*. Development in Soil Science 10. Elsevier Scientific, Amsterdam, 557 p.

Zanchi, C., Torri, D., 1980. *Evaluation of rainfall energy in central Italy*. In: De Boodt, Gabriels, D. (Eds.), *Assessment of Erosion*. Wiley, London, 133-142.

Zangger, E., 1991. *Prehistoric Coastal Environments in Greece: The Vanished Landscapes of Dimini Bay and Lake Lerna*. Journal of Field Archaeology 18 (1), 1-15.

Zelilidis, A., Kontopoulos, N., Piper, D.J.W., Avramidis, P., 1998. *Tectonic and sedimentological evolution of the pliocene-quaternary basins of Zakynthos island, Greece: Case study of the transition from compressional to extensional tectonics*. Basin Research 10(4), 393-408.

### Appendices

#### Appendix I: Laboratory Analysis

##### Grain size Analysis

Grain size analyses were carried out on 59 samples, based on a method by Konert & Vandenberghe (1997). The samples weighted 4 to 5 grams.  $\text{CaCO}_3$  was removed by addition of 10 ml 32% HCl. Distilled water (30 ml) was added, followed by half an hour of stirring. To remove organic material 25 ml 30%  $\text{H}_2\text{O}_2$  was added. Distilled water (50 ml) was added, followed by four hours of stirring. In cases of excess organic matter content samples were first sieved before cooking. The samples were boiled until all  $\text{H}_2\text{O}_2$  was removed from the solution. The samples were filled up to 800 ml with distilled water and left standing overnight to settle. The next day after decantation, 300 mg of  $\text{Na}_4\text{P}_2\text{O}_7 \cdot 10\text{H}_2\text{O}$  was added to separate clay minerals through peptisation followed by one minute of cooking. The remaining particles were injected into a laser analyser (Malvern Mastersizer 2000). Diffraction of laser beams by soil particles allows the analyser to calculate grain sizes.

##### CaCO<sub>3</sub> determination

The amount of  $\text{CaCO}_3$  was determined for 106 samples.  $\text{CaCO}_3$  was determined using a Scheibler calcimeter. Per sample 0.250 gr was put into an Erlenmeyer. Distilled water (15 ml) was added and a small plastic bottle filled with HCl (10 ml; 5%) was put into the Erlenmeyer. The Erlenmeyer was attached to a closed system. The small bottle of HCl was thrown over inside the Erlenmeyer. This causes a reaction between HCl and  $\text{CaCO}_3$  to form  $\text{CO}_2$ . The amount of  $\text{CO}_2$  released by this reaction is measured, being indicative for the amount of  $\text{CaCO}_3$  in the sample. The result of each sample is compared to the result of 0.25 gr pure  $\text{CaCO}_3$  allowing calculation of percentage  $\text{CaCO}_3$  for each soil sample.

##### Organic material Determination

The amount of organic material was determined for 106 samples through loss on ignition. A sample of 1-3 grams was put in a little ceramic basket. The basket was put in a stew (105 °C) for one day to remove remaining water. The sample was then put into an oven (450 °C) for 4 hours to remove organic material. The samples were weighted to a thousandth gram before stewing, between stew and oven and afterwards. The differences in weight allow calculation of water content and organic material content.

Appendix II: ArcGIS Model

All equations in the Morgan-Morgan-Finney model were carried out using ArcGIS. Equation 1 till 13 were done using the raster calculator in ArcGIS. Equation 14 was done using the Model Maker in ArcGIS. Equation 14 estimates the total runoff per year in mm flowing through a raster cell. The runoff model takes into account runoff from precipitation, runoff from upstream raster cells and infiltration along the slopes.

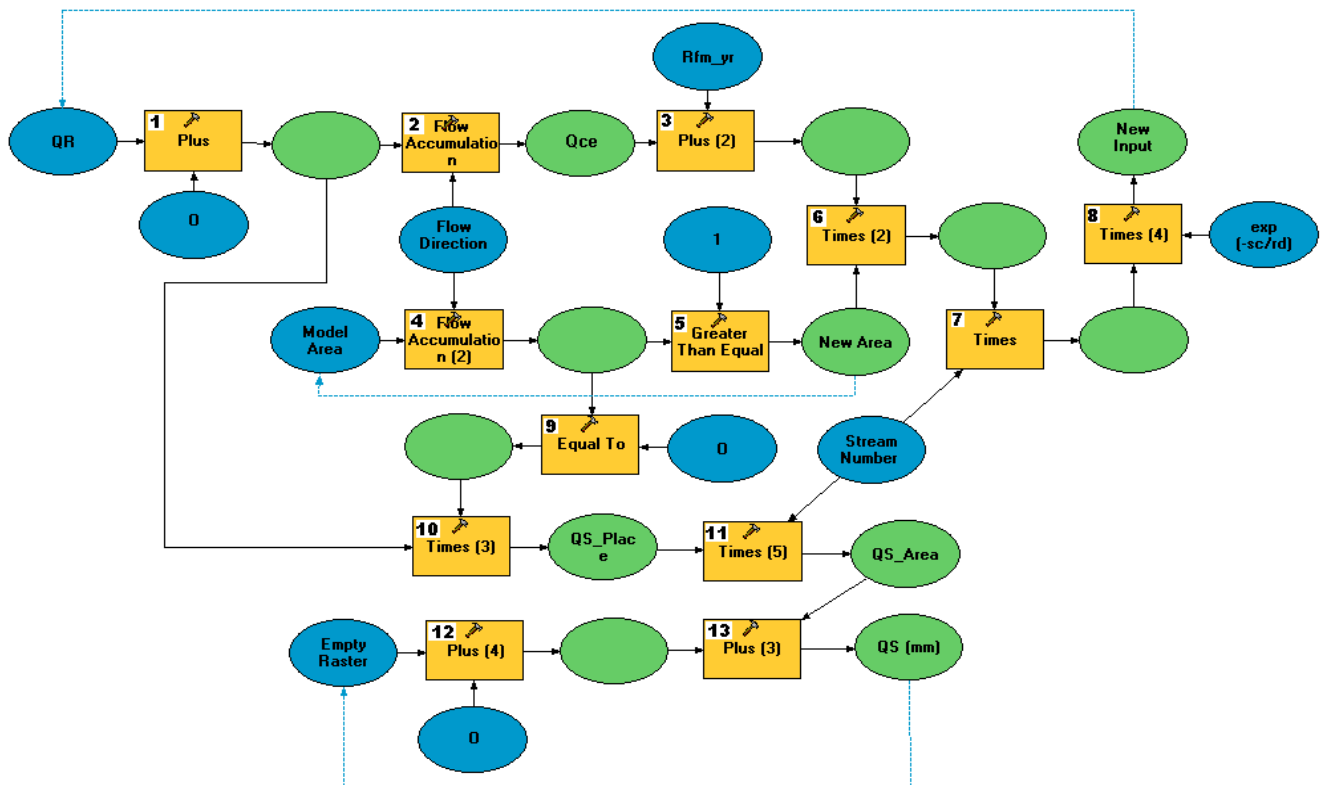


Figure 20: Runoff part of MMF-model in ArcGIS model maker. Blue circles represent input maps, green circles calculation results and the yellow squares are calculation steps.

The runoff part of the MMF-model is visualized in figure 20 and consists of 13 steps:

1. Plus 0: A necessary step to receive the right outputs.
2. Flow Accumulation: *Flow accumulation* calculates all the runoff received from upstream for all raster cells according to the local drainage pattern. This means the drainage divides get value 0 after the first iteration. The first cell directly underneath the drainage divide gets the value of solely the drainage divide cell, which is the runoff from upstream ( $Q_{ce}$ ).
3.  $Rfm_{yr}$  is added to all raster cells in the research area.
4. The model area input raster represents all cells that are taken into account. Using flow accumulation on the model area the cells that are "emptied" in step 2 are also emptied here.

5. The raster cells that are not “empty”, meaning their  $QS$  has not been added to the cells downstream, have a value of 1 or higher.
6. The raster cells that have to be taken into account for the next model iteration are separated from the cells that have been “emptied”. The cells that were 0 prior to step 3 become 0 again.
7. During every model run raster cells with the same stream order number get estimated. Why is explained later on.
8. The remaining raster cells, resembling  $QR$  plus  $Qce$ , are multiplied with  $\exp(-SC/RD)$  (equation 14). This becomes the new input for the next model iteration.
9. The raster cells with value 0 after step 4 are the cells which values have to be stored. The raster cells with value 0 get value 1, while all other cells get 0.
10. The raster cells with value 0 after step 9 are multiplied with  $QR (+ Qce)$ .
11. Only the raster cells with the correct stream order number are taken into account. Why is explained later on.
12. See step 1.
13. The  $QS$  values of the raster cells that are “emptied” during the model iteration are added to a raster in which all raster cells have value 0. This becomes the  $QS$  – map.

The stream order numbers are determined using the method of Shreve (1967). It is necessary to indicate the tributaries that need to be calculated using the stream order number (can be derived using the *stream order* tool in spatial analyst). If this is not done in the current model setup shorter tributaries are not taken into account when estimating  $QS$  in the main stems.

The change in stream order numbers have to be done manually along with some other changes. This makes the model in the current setup unusable for large catchments. The following steps have to be taken:

- Determine the area with for example stream order number = 1. This becomes the new input for the “Stream Order”-input map.
- Use the *expand* tool on the Stream Order-map (nr. Of cells: 1, zone values: 1) to get the new “Model Area”-input map.
- Multiply the new “Model Area”-input map with the final  $QS$  – map of the previous stream order number to receive the new input map for the next model runs.

The number of model iterations has to be the same as the longest tributary with the same stream order number.

Equation 15, 16 and 17 were done using the raster calculator. Equation 18, 19 and 20 are fitted in a model by using ArcGIS Model Maker. The erosion/deposition part of the MMF-model consists of 24 steps (figure 21):

1. Plus 0: A necessary step to receive the right outputs.
2.  $E$  minus  $TC$ .
3. If  $E$  minus  $TC$  is below 0 than  $E < TC$ .
4. If  $E$  minus  $TC$  is above 0 than  $TC < E$ .
5. For these raster cells  $E$  is  $E\_Out$ .
6. For these raster cells  $TC$  is  $E\_Out$ .
7.  $E\_Out$  of the calculated raster cells.
  
8. See step 1.
9. The model area input raster represents all cells that are taken into account. Using flow accumulation on the model area the cells that are "emptied" are separated from the cells which still have to supply their  $E\_Out$ .
10. The cells which are still active get value 1; the "empty" cells get value 0. The output is the new "Model Area" input-map.
11. All cells which are emptied get value 1.
12. Only the raster cells which get emptied during this iteration keep their value, all other raster cells are 0.
13. Only the raster cells with the correct stream order number are taken into account.
14. Using flow accumulation  $E\_In$  is calculated for the cells directly downstream the remaining cells from equation 13.
15.  $E$  is added to all cells in the area.
16. Only the raster cells which haven't been emptied yet keep their value, all other cells become 0. The output becomes the new input for  $E$  in the next model iteration.
  
17. The raster cells which haven't been emptied yet receive value 1, empty cells get the value 0.
18. The cells with value 1 from step 17 are multiplied with  $E$ .
19.  $E (+E\_in)$  minus  $E$ .
20. Only the raster cells with the correct stream order number are taken into account.
21. The remainder of step 20 minus  $E\_Out$ .
22. Only the cells that are emptied this step are taken into account.
  
23. See step 1.
24. Addition to a raster map with all cells 0 gives the erosion/deposition map.



Appendix III: The archaeological data

Archaeological survey was performed by bachelor students of the University of Amsterdam. The basic analytical unit of the survey team was the tract. The tract is defined as a visually homogenous area, bordered by topographical features such as stone walls. In tracts field walkers were placed every 5 meters. Field walkers recorded artefact quantities with a hand tally while walking in a straight line. During the return walk finds were collected. In this way 40% of the total artefact amount in a tract is documented after which total artefact quantities per tract were calculated (van Wijngaarden, 2006). These tracts are put into a GIS-environment visualizing the spatial distribution of archaeological material and the (probable) archaeological periods (figures 22 to 27).

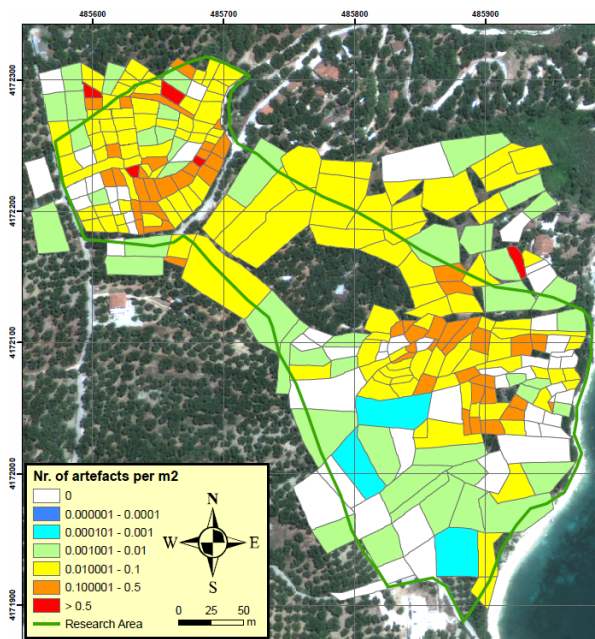


Figure 22: Amount of artefacts per m<sup>2</sup>.

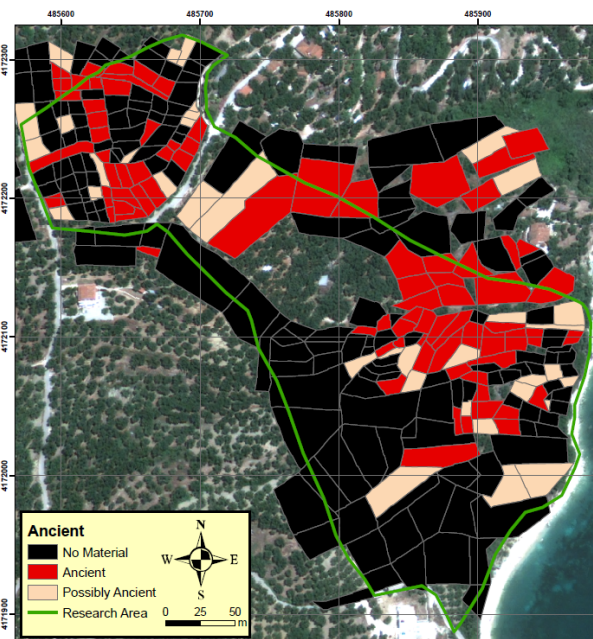


Figure 23: Ancient artefacts (older than 500 AD)

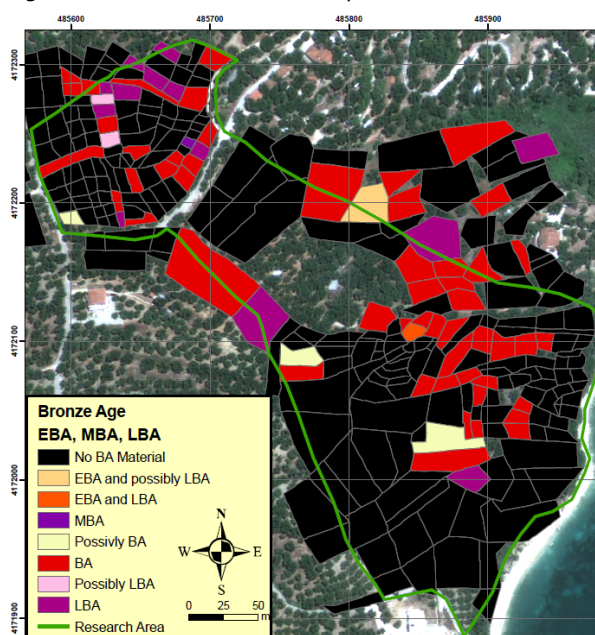


Figure 24: Bronze Age artefacts. EBA (5 - 4 cal kyr BP), MBA (4 - 3.6 cal kyr BP) and LBA (3.6 - 3.1 cal kyr BP) stand for respectively Early, Middle and Late Bronze Age.

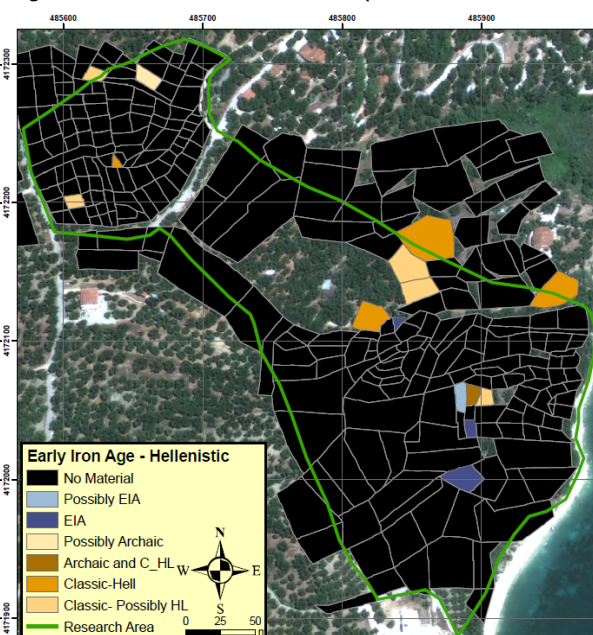


Figure 25: Early Iron Age (EIA; 3.1 - 2.7 cal kyr BP) until Hellenistic (HL; 330-146 BC) artefacts. Archaic material is from the period 700-480 BC. C stands for classical material (480-330 BC).

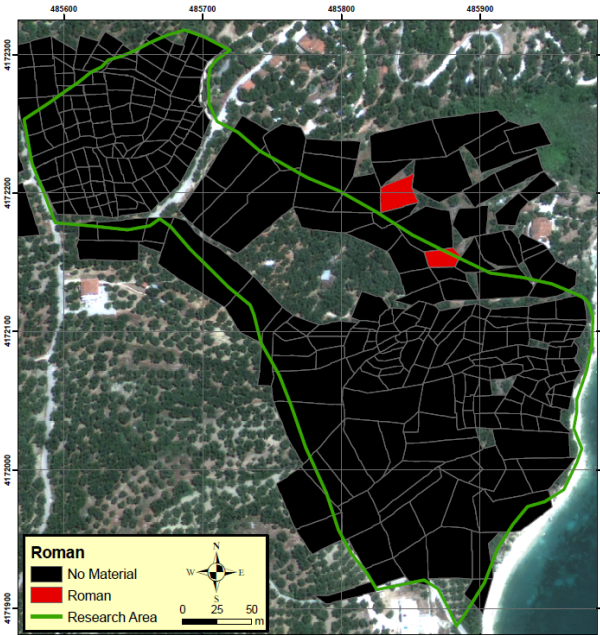


Figure 26: Roman artefacts (146 BC - ± 400 AD).

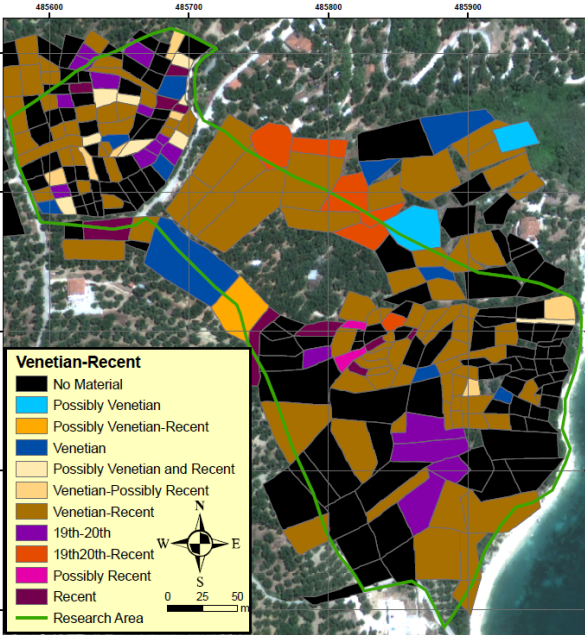


Figure 27: Venetian (1458-1900 AD) until Recent artefacts.

